Muscle-derived Myoglianin regulates *Drosophila melanogaster* imaginal disc growth

Ambuj Upadhyay[1], Aidan J. Peterson[1], and Michael B. O'Connor [1#]

[1]Department of Genetics, Cell Biology and Development
University of Minnesota
Minneapolis, MN 55455

Corresponding author

Michael B. O'Connor
Department of Genetics, Cell Biology and Development
6-160 Jackson Hall
Minneapolis, MN 55455
Tel. 612-626-0642
Email: moconnor@umn.edu

ABSTRACT

Organ growth and size are finely tuned by intrinsic and extrinsic signaling molecules. In *Drosophila,* the BMP family member Dpp is produced in a limited set of imaginal disc cells and functions as a classic morphogen to regulate pattern and growth by diffusing throughout imaginal discs. However, the role of TGFβ/Activin-like ligands in disc growth control remains ill-defined. Here we demonstrate that Myoglianin (Myo), an Activin family member, and a close homolog of mammalian Myostatin, is a muscle-derived extrinsic factor that uses canonical dSmad2 mediated signaling to regulate wing size. We propose that Myo is a myokine that helps mediate an allometric relationship between muscles and their associated appendages.

INTRODUCTION

How organ growth is regulated to achieve proper scaling with final body size has been a long standing question in developmental biology. Organ growth is a dynamic process that is finely tuned by highly conserved signaling molecules that are produced and act within the tissue of origin (intrinsic) or on a distant tissue (extrinsic) (Boulan et al., 2015; Hariharan, 2015; Johnston and Gallant, 2002; Mirth and Shingleton, 2012). These growth signals regulate final organ size through three distinct processes: cell division (proliferation), mass accumulation (cell growth) and cell death (apoptosis). The *Drosophila* wing imaginal disc, the larval precursor to adult wings and thorax, has been widely used as a model to study the molecular mechanisms that control organ growth and size control (Martin et al., 2009). Genetic analysis has identified numerous wing disc intrinsic factors, such as Wnt, Hedgehog, and Bone Morphogenetic Protein (BMP) homologs, that are required for proper patterning and proliferation (Hariharan, 2015). In contrast, examples of extrinsic factors that regulate imaginal disc growth are limited. The Insulin-like signaling pathway is one clear exception. Insulin-like peptides are produced in the brain and fatbody and are well known to promote both growth and proliferation in many tissues including imaginal disc cells (Boulan et al., 2015; Droujinine and Perrimon, 2013; Grewal, 2012; Nijhout, 2003; Shingleton et al., 2007; Sopko and Perrimon, 2013; Teleman, 2009). Insulin-like factors act in a physiological capacity to coordinate overall organismal growth with nutrition. Identification of other extrinsic growth signals could provide new insights into mechanisms governing coordinated organ scaling.

The largest and most diverse group of signaling molecules is the Transforming Growth Factor β (TGF-β) superfamily of growth and differentiation factors. The superfamily is subdivided into the BMP and the Activin/TGF-β-like subfamilies based on sequence and signaling relationships. In higher vertebrates, these growth factors play a myriad of roles during development from cell fate specification and stem cell maintenance to control of cellular growth and proliferation (Morikawa et al., 2016). Both branches of TGF-β are conserved in *Drosophila*, where limited functional redundancy and a powerful

genetic toolkit provide an attractive system for study (Peterson and O'Connor, 2014; Upadhyay et al., 2017). The *Drosophila* BMP ligand Decapentaplegic (Dpp) functions as a classic intrinsic morphogen, since it is secreted from a limited number of imaginal disc source cells and then diffuses throughout the tissue, to regulate proliferation and patterning based on its concentration gradient (Campbell and Tomlinson, 1999; Lecuit et al., 1996; Restrepo et al., 2014). Conversely, the Activin-like branch also plays a significant role in disc growth, however it is much less characterized (Brummel et al., 1999; Hevia and de Celis, 2013; Hevia et al., 2017).

In *Drosophila* Activin-like signaling is initiated by the three ligands, Myoglianin (Myo), Activinβ (Actβ), and Dawdle (Daw). These ligands bind to and activate a hetero-tetrameric receptor complex on the cell membrane consisting of two type-I receptor subunits encoded by the *baboon (babo)* locus and two type-II receptor subunits encoded by either the *punt* or *wishful-thinking (wit)* genes or perhaps a combination of the two (Upadhyay et al., 2017). Activated Babo phosphorylates cytosolic dSmad2 which then accumulates in the nucleus and, along with the co-Smad Medea, regulates expression of target genes (Brummel et al., 1999; Hevia et al., 2017). Notably, there are three splice isoforms of *babo* with different ligand binding domains, which presumably provide ligand binding specificity (Jensen et al., 2009). *Babo* null mutants die at the larval-pupal transition and have significantly smaller wing imaginal discs, and escapers produced by hypomorphic alleles also have smaller adult wings (Brummel et al., 1999). Conversely, expression of constitutively activated Babo in wing imaginal discs leads to larger adult wings that contain more cells, suggesting that Activin-like signaling has a role in regulating proliferation (Brummel et al., 1999; Hevia and de Celis, 2013). Additionally, Babo can signal non-canonically through Mad (the BMP Smad) to stimulate wing disc overgrowth, but only in the background of a protein null allele (Peterson and O'Connor, 2013).

For both the dSmad2 canonical and the Mad non-canonical signaling pathways, it remains unclear which Babo isoform and which Activin-like ligands, or combination thereof, regulates disc growth, nor is it clear which tissue(s) provide the ligands that promote disc growth. Expression analysis by *in-situ*

hybridization or RNAseq data suggests that all Activin-like ligands are expressed in the imaginal wing disc, albeit at low levels, perhaps indicating collective contribution to stimulating tissue growth (Graveley et al., 2011; Hevia and de Celis, 2013). However it is important to recognize that mRNA expression does not necessarily correlate with secretion of functional ligand, especially since TGF-β–type ligands undergo a series of post-translational modifications and ligand processing to generate active molecules, and these processes may vary within different tissues (Akiyama et al., 2012).

Here we report our analysis of Activin-like ligands and Baboon isoforms for their roles in regulating imaginal disc growth. Through a series of genetic experiments, we demonstrate that among the three *Drosophila* Activin-like ligands, only Myo is required for proper growth of imaginal discs. We also identify the receptors Babo-A and Punt along with the co-factor Plum as being necessary for Myo regulation of wing imaginal disc growth via phosphorylation of dSmad2. Surprisingly, we identify the tissue source of Myo that controls disc growth to be the larval muscle.

RESULTS

Myoglianin is required for proper disc growth

All *Drosophila* Activin-like ligands (Myo, Actβ, and Daw) have tissue specific function yet signal via the sole Type-I receptor Babo. Hence, the *Babo* mutant phenotype is likely a composite of the three individual ligand mutant phenotypes. The imaginal discs of *Babo* mutants are approximately 30% smaller than wild-type but do not exhibit any obvious defects in tissue patterning (Brummel et al., 1999). We set out to identify which Activin-like ligand(s) are required for proper imaginal disc growth. Null *myo*, *actβ,* and *daw* mutants are larval or pharate lethal (Awasaki et al., 2011; Ghosh and O'Connor, 2014; Zhu et al., 2008). Therefore, we analyzed the size of imaginal wing discs from late 3rd instar larvae of null mutant animals. For this initial analysis, we used a simple yeast/sugar diet (5Y5S), because *daw* mutants are sensitive to standard acidic cornmeal food (Ghosh and O'Connor, 2014). Interestingly, only

myo mutants yield small discs, phenocopying *babo* mutants. *Myo* wing discs are approximately 40% smaller than *yw* controls, but retain their normal shape and pattern (Fig 1 B,E). *Actβ* mutant discs had no significant size defects, however *daw* mutant discs were slightly smaller, which may be attributable to the reduction of insulin secretion in the *daw* mutants (Fig 1 C-E) (Ghosh and O'Connor, 2014). Previous studies suggested that all Activin-like ligands are expressed in the wing disc (Hevia and de Celis, 2013). Despite this observation, our result clearly suggests that only *myo* is functionally required for growth of the discs, and that other ligands may have other functions apart from disc growth. We next asked whether other imaginal tissues such as the haltere and leg discs are also affected by the loss of *myo*. Indeed, both these imaginal discs are also approximately 40-50% smaller in *myo* mutants and maintain their proportional size (Fig 1F-I). This suggests that Myo signaling regulates tissue growth in all three of these imaginal discs to similar extents.

To determine why *myo* mutant discs are small, we measured cell size, cell growth, proliferation, and apoptosis. First, to assess cell size, we used phalloidin staining to mark the apical actin belt, and measured the apical surface area of disc epithelial cells and found that wing disc cells of *myo* mutants are 22% smaller than controls (Fig J-L). Next, we examined proliferation by staining for phospho-Histone 3(ser10) to mark mitotic cells, and found no significant difference between *myo* discs and controls at mid L3 stage (Fig 1, M-O). Third, using the apoptotic marker cleaved-caspase 3, we found no increase in apoptosis in *myo* mutants at the early L3 stage (Fig S1 A-B).

Another possible explanation for why *myo* mutant discs do not grow properly is TOR pathway regulation. To address this, we stained growing early L3 imaginal discs for phospho-S6, which is a target of pS6k and a readout of TOR pathway activation (Romero-Pozuelo et al., 2017). We find no decrease in pS6 staining in *myo* mutant discs, indicating that TOR signaling is not perturbed in these cells (Fig S1 C-D). To summarize, *myo* mutant discs are smaller in part due to smaller cells. However, the 22% decrease in cell size is insufficient to completely account for the 40-50% decrease in total tissue size. Because our proliferation and apoptosis assays are snapshot experiments of fixed tissues, we conclude that the portion

of final disc size that cannot be accounted for by smaller cell size represents either a small proliferation reduction or a slight increase in apoptosis rate that cannot be detected at individual time points but over the course of the entire developmental period leads to an additional ~20% decrease in disc size.

Myo is homologous to vertebrate *Mstn*, which negatively regulates skeletal muscle size by inhibiting proliferation of muscle stem cells (Morikawa et al., 2016) and regulation of protein homeostasis (Lee et al., 2011; Rodriguez et al., 2014; Trendelenburg et al., 2009). Recent studies in *Drosophila* using RNAi tissue specific knockdown suggested that Myo also functions as a negative regulator of muscle size similarly to vertebrate *Mstn* (Augustin et al., 2017). We re-examined this issue using *myo* null alleles. Surprisingly, we find that larval muscles #6 and #7 (Segment A2) at the late L3 stage contain the same number of nuclei, indicating no defects in myoblast fusion during embryogenesis, yet they are 13% smaller than heterozygous controls (Fig1 P-S). We conclude that with respect to muscle size control, *myo* is not functionally conserved with vertebrate *Mstn*.

Myo signals canonically via dSmad2

Canonical TGF-β/Activin pathway activation in *Drosophila* is mediated by C-terminal phosphorylation of dSmad2 by the Type-I receptor Baboon (Brummel et al., 1999; Peterson and O'Connor, 2014; Upadhyay et al., 2017). To determine if Myo acts through the canonical signaling pathway, we examined phosphorylated dSmad2 (p-dSmad2) levels in wing disc extracts of various mutants. Wing disc extracts of late L3 larvae from *yw*, *myo* heterozygotes and null animals were Western blotted and probed with anti phospho-dSmad2 (p-dSmad2) antibody. We observe a dose dependent reduction in p-dSmad2 levels upon loss of *myo*, i.e. in heterozygous *myo*$^{-/+}$ the p-dSmad2 signal is reduced compared to wild-type, whereas in homozygous null mutants there is no signal under our detection conditions. These findings indicate that Myo provides the majority of canonical signal to the wing disc. (Fig1 T-U).

Myo signaling in imaginal discs requires a specific isoform of Baboon

Baboon is the sole Activin branch Type I receptor in *Drosophila*, but encodes three splice isoforms (Awasaki et al., 2011; Jensen et al., 2009). The three splice isoforms are a result of mutually exclusive alternative splicing of the fourth exon (4a, 4b, 4c) giving rise to three receptors (Babo-A, Babo-B, and Babo-C) (Brummel et al., 1999; Jensen et al., 2009) that differ only in their extracellular, ligand binding domains. It has been suggested that different tissues express different isoforms, perhaps in order to tune tissue-specific responses to various ligands (Awasaki et al., 2011; Jensen et al., 2009). Ectopic Myo expression in the larval brain is lethal, however viability can be partially restored by simultaneously knocking down Babo-A but not Babo-B or Babo-C (Awasaki et al., 2011). These findings suggest that Myo signals specifically via Babo-A. Since only *myo* is required for proper growth of imaginal discs (Fig1 B), we reasoned that Babo-A should be the major Babo isoform expressed in the discs, a conjecture confirmed by qPCR analysis of dissected late L3 wing discs (Fig.2-A). We verified that our primers for Babo-B and Babo-C are functional by testing other tissues such as carcass, brain, and fat body where we find different profiles for each isoform. (Fig. S2).

To confirm that the Babo-A isoform is indeed required for wing growth, we employed the GAL4/UAS system to conduct tissue and isoform-specific RNAi knockdown experiments. Using *esg* (entire disc), *ci* (anterior), and *hh* (posterior) GAL4 lines, we knocked down specific Babo isoforms and measured overall tissue size and cell size/density. In support of the qPCR data, we find that knocking down Babo-A alone with *esg-GAL4* results in 40% smaller adult wings, whereas knocking down Babo-B or Babo-C resulted in no size difference (Fig.2 B-E, J). *Ci-GAL4* driving *babo-a* RNAi reduces the anterior compartment by 50% (Fig.2 F-I, L). In other experiments, we verified that the *babo-b* and *c* isoform specific RNAis are functional and produce phenotypes, thereby indicating that lack of wing phenotype by knockdown with these isoforms is not due to poor efficiency of

these RNAis.

We next assessed cell size in these wings by measuring trichome density in adult wings. RNAi for *babo-a* using *esg-GAL4* or *ci-GAL4* results in a fractional decrease (-6%) or increase (12%) in cell density respectively (Fig.2 K, M) indicating that the *esg* driver results in larger cells whereas the *ci* driver results in smaller cells. Assuming no difference in the number of wing disc precursors after embryogenesis, we infer that the *esg* driver leads to smaller wing size (Fig.2 C) due to defects in proliferation, whereas, in the case of the *ci* driver, the smaller compartment size (in Fig.2 G) is due to both smaller cells and fewer cell divisions. As a further test, we repeated the experiment with *hh-GAL4* which is expressed in the posterior compartment. Knockdown of *babo-a* using the *hh* driver is pupal lethal, thus we analyzed the late L3 imaginal wing discs. At this stage, in addition to the predicted smaller posterior compartment (-35%, Fig.2 P), we observe two additional phenotypes that are obscured in adult wings. Knockdown of *babo-A* results in an imperfect anterior/posterior boundary formation (Fig.2 N-O) as well as a 40% decrease in epithelium thickness (Fig.2 Q). Taken together, this set of experiments demonstrates that Babo-A is the only functional isoform in the wing imaginal disc, and loss of *babo-a* phenocopies *myo* mutants in regulating wing disc growth. Thus, similar to the mushroom body neurons (Awasaki et al., 2011), our data demonstrate that Myo signals solely through Babo-A in the wing imaginal disc.

Babo-A, Punt, and Plum mediate non-canonical signaling in wing imaginal discs

In addition to canonical signaling, Babo can also signal non-canonically by cross-talk with downstream components of the BMP/Dpp pathway (Peterson and O'Connor, 2013). Non-canonical Babo activity is only detectable in a protein null mutant of *dSmad2* or a strong RNAi knockdown of *dSmad2* (Peterson and O'Connor, 2013; Peterson et al., 2012; Sander et al., 2010). In the absence of its preferred target dSmad2, Babo promiscuously activates Mad, the BMP ortholog of dSmad2, which then represses

brk expression throughout the disc leading to overgrowth of the tissue along the anterior-posterior axis (Peterson and O'Connor, 2013). We hypothesized that the non-canonical signaling is mediated by Babo-A and not via other isoforms ectopically signaling in the absence of *dSmad2*. Babo activation can be visualized in *dSmad2* loss-of-function clones using the *brk* (*B14-LacZ)* reporter (Müller et al., 2003; Peterson and O'Connor, 2013). We used this assay to generate *dSmad2* RNAi clones and confirmed the ectopic *brk-LacZ* silencing (Fig. 3A). Next, we performed genetic epistasis analysis by simultaneously knocking down *dSmad2* along with each of the *babo* isoforms in clones and then assayed for *brk-LacZ* rescue. Knocking down *dSmad2* and *babo-a* rescued *brk* reporter expression (Fig. 3 A vs B), while RNAi of *dSmad2* and *babo-b* or *babo-c* did not (Fig. 3 A vs C-D). To further test if non-canonical activity of Babo-A occurs throughout the wing disc, we knocked down *dSmad2* in the entire disc using *esg-GAL4*, resulting in disc overgrowth which can be quantified by measuring the height/width ratio of the disc-pouch (Fig. S3 A-B) (Peterson and O'Connor, 2013; Sander et al., 2010). RNAi for *dSmad2* alone results in the H/W ratio dropping from 0.91 (ctrl, *esg>*) to 0.66 (*esg>idSmad2*) (Fig. S3 D-E). Epistasis analysis with specific *babo* isoforms demonstrates that only RNAi of *babo-a*, and not *babo-b* or *babo-c*, suppresses the widening induced by *dSmad2* RNAi (Fig. S3). Taken together, these experiments suggest that Babo-A is the sole signaling receptor in the wing imaginal disc mediating both canonical and non-canonical signaling.

TGFβ signaling requires ligands binding to hetero-tetrameric type-I and type-II receptor complexes. There are two type-II receptors in the *Drosophila* genome: *punt* and *wishful thinking* (*wit*), both of which can signal with Type-I receptors from either branch of the TGFβ superfamily (Upadhyay et al., 2017). Punt is more commonly utilized during development, and facilitates Dpp signaling in the wing imaginal disc in combination with the BMP type I receptors Tkv and Sax (Brummel et al., 1994; Fuentes-Medel et al., 2012; Letsou et al., 1995; Parker et al., 2006). In cell culture models however, Punt can also signal in combination with Babo and Activin-like ligands (Brummel et al., 1999; Jensen et al., 2009; Letsou et al., 1995). Conversely, Wit functions primarily at the neuromuscular junction with the BMP

ligand Gbb (Marqués et al., 2002) although it has been shown to bind Myo in combination with Babo in mammalian cell culture (Lee-Hoeflich et al., 2005). Since both *punt* and *wit* are expressed in the wing imaginal disc, it is unclear whether one or both type II receptors are required for Myo-Babo signaling (Childs et al., 1993; Marqués et al., 2002). To address this issue we utilized the *brk* silencing assay in RNAi clones as described above. We find that while RNAi for *punt* suppress the *dSmad2* induced *brk* silencing (Fig. 3 E vs G), RNAi for *wit* does not suppress *brk* silencing in the same context (Fig. 3 E vs F). Taken together, these experiments demonstrate that Babo-A requires Punt, but not Wit, for proper control of *brk* expression in this non-canonical wing disc signaling assay and leads us to conclude that Myo and Babo-A signal with Punt to control normal wing disc growth.

In addition to Type-I and Type-II receptors, various additional co-receptors have been found to interact with TGF-β ligands and receptors to facilitate signaling (Heldin and Moustakas, 2016). *Drosophila plum* encodes an immunoglobulin superfamily protein, and is required for Myo stimulated pruning of mushroom body neurons (Yu et al., 2013). Therefore, we examined whether *plum* also facilitates Babo activity in the context of wing imaginal disc growth. Indeed, we find that *plum-RNAi* in the wing disc rescues the *dSmad2* mutant overgrowth phenotype, confirming that Plum is required for Myo/Babo signaling in the wing disc similar to its requirement in mushroom body neurons (Fig. S4). This observation together with the previous report (Yu et al., 2013) suggest that Plum may be widely utilized as a co-receptor for Myo/Babo signaling in *Drosophila*.

Muscle-derived myoglianin signals to the wing disc

Growth factors such as Wg and Dpp are tissue intrinsic ligands, produced by and acting on the wing disc cells. We sought to determine the source of Myo that signals to the imaginal discs. The name *myoglianin* refers to the two tissues (muscles and glia) in which myo expression was initially observed (Lo and Frasch, 1999). More recent RNA *in situ* hybridization results suggest that *myo* is expressed in the wing imaginal disc at low levels (Hevia and de Celis, 2013). To precisely determine the source of Myo that acts on the wing disc, we first examined the expression pattern of *myo* in late L3 larvae using *myo-*

GAL4 reporter to drive *UAS-CD8-GFP* (Awasaki et al., 2011). We detect GFP expression in both the glial cells of the brain and the ventral ganglia, as well as the larval body wall muscles (Fig. 4 A-B), but we do not observe any GFP signal in any imaginal discs (Fig. 4 A). Thus, we conclude that either *myo* is not expressed in the wing disc or that our *myo-GAL4* construct does not include all of the endogenous enhancers.

To determine the functional source of Myo that controls imaginal disc growth, we conducted loss-of-function studies in the *dSmad2* null mutant background, and looked for rescue of the wing disc overgrowth phenotype. First, using null mutant alleles, we confirmed that loss of *myo* in *dSmad2* mutant background suppress the *dSmad2* overgrowth, resulting in small discs similar in size to *myo* mutants (Fig. 4 C-E). Next, we knocked down *myo* using tissue specific GAL4 drivers. To confirm efficacy of the RNAi constructs, we first used the *da-GAL4* driver to ubiquitously knock down *myo* in the *dSmad2* background and confirmed that it suppresses wing disc overgrowth (Fig. 4 F vs G). Next, knocking down *myo* using either *esg-GAL4* (wing disc) or *repo-GAL4* (glia) failed to suppress the *dSmad2* wing disc overgrowth (Fig. 4 F vs H-I). This result suggests that the wing discs are receiving a strong Myo signal even when knocked down in the imaginal discs or glia. In contrast, RNAi for *myo* in body wall muscles, using either *mhc-GAL4* or *mef2-GAL4* drivers, completely suppresses the *dSmad2* disc overgrowth phenotype phenocopying the *dSmad2;myo* double mutant (Fig. 4 F vs J-K). Therefore, we conclude that muscles are the major source of Myo that stimulates imaginal disc growth.

Overexpression of Myo in muscle or fat body rescues *myo* mutant disc growth

While the suppression of disc overgrowth in a *dSmad2* mutant background strongly implicates muscle as the source of ligand, we also examined if Myo expression in muscle, or other non-disc tissues, could rescue the size of *myo* mutant discs. First ubiquitous overexpression of *myo* in wild type larva results in wings that larger than normal (Fig. S5). Next, we examined whether overexpression of *myo* in either glia, muscles, or fat body is able to rescue size of *myo* mutant discs. Overexpression in glia (*repo-GAL4*) results in partial rescue (Fig. 5 C, F) while overexpression in muscle (*Mef2-GAL4*, Fig. 5 D, F) or

fat body (*cg-GAL4*, Fig 5 E, F) leads to complete rescue. These results clearly demonstrate that Myo produced in distant tissues can signal to wing discs, albeit with varying degree of signaling strength depending on the source. Collectively, these results indicate that muscle-derived Myo acts as an endocrine-like ligand via the hemolymph to activate a specific receptor complex on disc cells, consisting of Babo-A, Punt and Plum, that signals to dSmad2 to promote imaginal disc growth.

DISCUSSION

Understanding the physiologic roles of inter-organ signaling during development is an emerging and complex field. In particular, how and which inter-organ signals regulate organ/tissue growth remains an open question. In the present study, we demonstrate that the *Drosophila* Activin-like ligand Myoglianin is a myokine that acts systemically to fine tune imaginal disc growth. We suggest Myo tuning of disc growth may play an important role in maintaining proper allometric scaling of appendage size with the size of the muscles that control their movements.

Only Myo regulates imaginal disc size

Although Babo/dSmad2 signaling has been previously implicated in imaginal disc growth control (Brummel et al., 1999; Hevia and de Celis, 2013; Peterson and O'Connor, 2013), the ligand(s) responsible and their production sites(s) have not been identified. Previous *in situ* hybridization and RNAi knockdown experiments suggested that all three Activin-like ligands (Myoglianin, Activinβ, and Dawdle) contribute to control of wing size (Hevia and de Celis, 2013). However, we find no expression in imaginal discs, with the exception of Actβ which is expressed in differentiating photoreceptors of the eye imaginal disc (Moss-Taylor et al., 2019; Zhu et al., 2008). More importantly, using genetic null mutants, we show that only loss of *myo* affects imaginal disc size. The discrepancy in phenotypes between tissue-specific knockdown results and the genetic nulls is often noted and not fully understood (Di Cara and King-Jones, 2016; Gibbens et al., 2011). In addition to simple off-target effects within the wing disc itself, one

possible explanation is that many GAL4 drivers are expressed in tissues other than those reported, potentially resulting in deleterious effects for the animal that indirectly affect imaginal disc size. Another possibility is that in *Actβ* and *daw* genetic null backgrounds a non-autonomous compensatory signal is generated by another tissue and this signal is not activated in the case of tissue-specific knockdown (Di Cara and King-Jones, 2016). We think both of these explanations are unlikely in this instance since we demonstrate that only the Babo-A receptor isoform is expressed and required in discs and we previously showed that Daw only signals through the Babo-C isoform (Jensen et al., 2009). Therefore, it is unclear why knockdown of *daw* in the wing disc would result in a small wing phenotype as previously reported (Hevia and de Celis, 2013). We conclude that the small wing phenotypes caused by RNAi knockdown of *Actβ* or *daw* are likely the result of off-target effects and that Myo is the only Activin-type ligand that regulates imaginal disc growth.

Plum and Punt are required for efficient Babo-A signaling to dSmad2 in the wing disc

The signaling ability of TGF-β ligands is modulated by the specific combinations of receptors and co-receptors to which they bind (Heldin and Moustakas, 2016). In *Drosophila*, the receptor requirements for effective signaling through dSmad2 likely vary for each ligand and tissue (Jensen et al., 2009). In this report, we find that Myo signaling in the wing disc requires Punt as the type II receptor, Babo-A as the type I receptor and Plum as a likely co-receptor. Furthermore, we establish that Myo is the exclusive Activin-like ligand signaling to the discs since loss of Myo eliminated detectable phosphorylation of dSmad2 in the wing imaginal disc. Since Babo-a is the only isoform expressed in wing discs we also conclude that Myo is able to signal through this isoform in the absence of other isoforms. Whether Myo can also signal through Babo-a or c is not yet clear, but in the context of mushroom body remodeling Babo-A also appears to be the major receptor isoform required (Awasaki et al., 2011; Yu et al., 2013). Plum is also required for mushroom body remodeling, suggesting that Plum and Babo-a are both required for efficient Myo signaling. However, it is noteworthy that Plum null

mutants are viable (Yu et al., 2013) while Myo null mutants are not. This observation suggests that Plum is not required for all Myo signaling throughout the animal.

The requirement of Punt as a type II receptor for production of an efficient signaling complex with Myo may be context dependent. In the mushroom body, indirect genetic evidence suggests that the two Type II receptors function redundantly (Zheng et al., 2006). Although both *punt* and *wit* are expressed in imaginal discs (Childs et al., 1993; Marqués et al., 2002), only loss of *punt* produces a phenotype in the *brk* reporter assay. The requirement of both Punt and Plum for Myo signaling may also explain why a previous attempt to study Myo signaling in a heterotypic cell culture model failed (Lee-Hoeflich et al., 2005). In that study, Myo was found to form a complex with Wit and Babo-a in COS-1 cells but no phosphorylation of dSmad2 was reported. One explanation is that effective signaling by Myo requires Punt, Plum, and Babo-A, and none of these is found in mammalian cells. Collectively, our results provide *in vivo* functional evidence for a Myo signaling network that regulates growth.

Proliferation and cell size

Final tissue size is determined by several factors including cell size, proliferation, death rates, and duration of the growth period. While we did observe cell size changes upon manipulation of Myo signaling, the direction of change depended on the genotype. In *myo* mutants, estimation of cell size via apical surface area indicates that the cells are ~20% smaller than wild-type. Although this measurement does not indicate the actual volume of the cells, it gives an indication of cell density in the epithelial sheet of the wing pouch, which is analogous to counting cells in the adult wing. RNAi knock down of *babo-a* in the entire disc produced smaller adult wings with larger (less dense) cells. This result differs from the *myo* mutant, but is similar to the reported adult wing phenotypes of *babo* mutants (Hevia and de Celis, 2013) and larval disc phenotypes of *dSmad2* mutants (Peterson and O'Connor, 2013). When *babo-a* is knocked down in one compartment, that compartment is reduced in size with smaller cells. We conclude that tissue size reduction is the consistent phenotype upon loss of Myo signaling, but cell size changes depend on the specific type of manipulation.

While cell size effects may be context dependent, it is notable that neither reduction in size of imaginal discs nor adult wing surface area can be explained solely by a cell size defect. Therefore, we believe that a subtle proliferation or apoptotic defect also contributes to the phenotype. Consistent with the possibility of a proliferation defect is the observation that the large disc phenotype exhibited by dSmad2 protein null mutants is clearly dependent on Myo, and we have previously shown that this is the result of enhanced proliferation (Peterson and O'Connor, 2013). Likewise, earlier studies showed that expression of activated Babo in wing discs also leads to larger wings with slightly smaller cells which is most easily explained by an enhanced proliferation rate (Brummel et al., 1999). It is worth noting that this proposed enhanced proliferation rate will be very difficult to detect since cell division is random with regard to space and time during development (Wartlick et al., 2011). Thus the final ~40% reduction in adult wing size translates to disc cells dividing on average 1 less time throughout the entire time course of larval development. Therefore, without prolonged live imaging, this small reduction in proliferation rate will not be detectable using assays that provide only static snap shots of cell division.

One attempt to shed light on the transcriptional output of TGF-β signaling responsible for wing disc size employed microarray mRNA profiling of wild-type versus *dSmad2* gain- and loss-of-function wing discs (Hevia et al., 2017). However this study did not reveal a clear effect on any class of genes including cell cycle components, and it was concluded that the size defect is the result of small expression changes of many genes Consistent with this view are dSmad2 Chromatin Immunoprecipitation experiments in Kc cells which revealed that dSmad2 is associated with many genomic sites and thus may regulate a myriad of genes (Van Bortle et al., 2015).

Is *myoglianin* function evolutionarily conserved?

Insect *myoglianin* is a clear homolog of vertebrate *Myostatin* (*Mstn/GDF8*) (Hinck et al., 2016), a TGF-β family member notable for its role in regulating skeletal muscle mass. *Mstn* loss-of-function

mutants lead to enlarged skeletal muscles (Grobet et al., 1997; McPherron and Lee, 1997). Mstn is thought to affect muscle size through autocrine signaling that limits muscle stem cell proliferation, as well as perturbing protein homeostasis via the Insulin/mTOR signaling pathways (Morikawa et al., 2016; Rodriguez et al., 2014). Similarly, *Gdf11*, a *Mstn* paralog, also regulates size and proliferation of muscles and adipocytes, and may promote healthy aging (Egerman et al., 2015; McPherron et al., 2009; Sinha et al., 2014). *Mstn* and *Gdf11* differ in where they are expressed and function. *Mstn* is highly expressed in muscles during development while *Gdf11* is weakly expressed in many tissues. Both molecules are found to circulate in the blood as latent complexes in which their N-terminal prodomains remain associated with the ligand domain. Activation requires additional proteolysis of the N terminal fragment by Tolloid-like metalloproteases to release the mature ligand for binding to its receptors (Uhlén et al., 2015; Wolfman et al., 2003). Interestingly in *Drosophila*, the Myoglianin N-terminal domain was also found to be processed by Tolloid-like factors, but whether this is a prerequisite for signaling has not yet been established (Serpe and O'Connor, 2006). In terms of functional conservation in muscle size control, however, the role of *Drosophila* Myo remains ambiguous. Analysis of the null mutant in the present study indicates that it has little effect on muscle size. However a recent study employing a muscle-specific RNAi knockdown of *myoglianin* (*myo*), reported finding larger muscles similar to the vertebrate observation (Augustin et al., 2017). This discrepancy between the tissue-specific RNAi knockdown and the null phenotypes is something that is found relatively frequently in both *Drosophila* and also in vertebrates and may represent activation of compensatory pathways in the null phenotype that are not triggered by tissue specific knockdown (Di Cara and King-Jones, 2016; El-Brolosy and Stainier, 2017; El-Brolosy et al., 2019; Gibbens et al., 2011). Interestingly, studies of *Mstn* homologs in shrimp suggests that it is required for proper growth of muscles (De Santis et al., 2011). Indeed, we find that loss of Actβ, another ligand that signals through Babo and dSmad2, results in a smaller muscles (Moss-Taylor et al., 2019) contrary to that produced by loss of vertebrate *Mstn* and various other vertebrate Activin family members. Thus, in arthropods, it appears that the Myo/Activin pathway is required to promote muscle growth, while in vertebrates they inhibit muscle growth. Whether arthropod Activin-like ligands promote muscle growth

by regulating Insulin/Tor signaling in the opposite direction compared to vertebrates remains to be determined.

Intrinsic (intra-organ) vs extrinsic (inter-organ) mode of Myo signaling and the significance of muscle to disc inter-organ communication

The most intriguing finding of this study is that muscle-derived Myo acts non-autonomously to regulate imaginal disc growth. This is in stark contrast to the two BMP ligands, Dpp and Gbb, which are produced by disc cells and act autonomously within the disc itself to regulate both growth and pattern (Haerry et al., 1998; Minami et al., 1999). The fact that a TGF-β ligand can act in an endocrine-like manner is not particularly novel since many vertebrate members of the TGF-β family, including Myostatin, the closest homolog to *Drosophila* Myoglianin, are found in the blood (Sinha et al., 2014). Even the disc intrinsic molecule Dpp has been recently shown to be secreted into the hemolymph where it circulates and signals to the prothoracic gland to regulate a larval nutritional checkpoint (Setiawan et al., 2018). Several additional reports indicate that ligands from the *Drosophila* Activin-like subfamily also circulate in the hemolymph and function as inter-organ signals. For example, muscle derived Actβ and Myo signal to the fat-body to regulate mitochondrial function and ribosomal biogenesis, respectively (Demontis et al., 2014; Song et al., 2017). In addition, Dawdle produced from many tissue sources can signal to the Insulin producing cells and the mid-gut to stimulate Insulin secretion and repress expression of sugar metabolizing genes, respectively (Chng et al., 2014; Ghosh and O'Connor, 2014). Thus many TGF-β type factors act as both paracrine and endocrine signals depending on the tissue and process involved.

The phenotype of the *myo* mutant animal supports our claim that endogenous Myo contributes to imaginal disc growth. The ectopic expression assay produced various wing disc sizes when Myo was expressed in different tissues, indicating that the growth response likely depends on the level of Myo being produced in the distal tissue. Loss of glial derived Myo is not sufficient to suppress overgrowth of

dSmad2 mutant discs, but overexpression of Myo in glia did partially rescue size of *myo* null wing discs, likely because the *repo*-Gal4 driven overexpression produces more ligand than endogenous glia. Likewise, expression from a large tissue such as muscle or fatbody likely produces more Myo than glia leading to normal disc growth or even overgrowth. It is also possible that Myo signaling activity is modified depending on the tissue source. Like other TGF−β family members, Myo requires cleavage by a furin protease at its maturation site to separate the C-terminal ligand from the prodomain (Lee-Hoeflich et al., 2005; Lo and Frasch, 1999), and Myo may also require a second cleavage by a Tolloid protease family member to achieve full dissociation of the prodomain from the ligand to ensure complete activation (Serpe and O'Connor, 2006). Either of these cleavage reactions, or any other step impacting the bioavailability of active Myo ligand, may vary with tissue or may be modulated by environmental conditions.

What is the rationale for larval muscle regulating imaginal discs size? A possible reason is that for proper appendage function, the muscle and the structure (leg, wing, and haltere) that it controls should be appropriately matched to ensure optimal organismal fitness for the environmental niche the adult occupies. For example, a large muscle powering a small wing might result in diminished fine motor control. Conversely, a small muscle may not be able to power a large wing to support flight. However, the multi-staged nature of muscle and appendage development complicates this picture. Larval muscles are histolysed during metamorphosis and do not contribute to the adult muscle. However, remnants of larval muscles in the thoracic segment are preserved as fibers that act as scaffolds upon which the larval myoblasts infiltrate and fuse to become the adult indirect flight muscles (Dutta et al., 2004). Thus, at least for the indirect flight muscles, the size of the larval muscle scaffold might contribute to the building of a bigger adult muscle. Another possibility invokes a signal relay system. Wg and Serrate/Notch signaling from the wing disc epithelial cells control myoblast proliferation during larval development (Gunage et al., 2014). Thus it may be that Myo signaling from the larval muscles stimulates proliferation of the disc epithelial layer which in turn enhances Wnt and Serrate/Notch signaling to myoblasts to increase their

number thereby coordinating the adult appendage size with muscle size. A final scenario is that, since muscle is a major metabolic and endocrine organ, Myo production may be regulated by the general metabolic state of the larva. If healthy, high levels of Myo, in concert with other growth signals such as insulin, leads to a bigger fly with large wings, and if the metabolic state is poor then lower Myo levels leads to diminished proliferation and a smaller cell size resulting in a smaller fly with small wings.

Regardless of the precise mechanism, the ability of the muscle to control appendage size has interesting implications in terms of evolutionary plasticity. The proportionality of insect wing size to body size can vary over a large range (Shingleton et al., 2008), but the mechanism responsible for determining this particular allometric relationship for a given species is not understood. We have recently demonstrated that in *Drosophila*, motoneuron derived Actβ, another TGF-β superfamily member, can dramatically affect muscle/body size (Moss-Taylor et al., 2019). Therefore, it is tempting to speculate that evolutionary forces might modulate the activity of these two genes to produce an appropriate body-wing allometry that is optimal for that species' ecological niche.

Figure Legends

Figure 1. *Myoglianin* regulates size of imaginal discs and activates dSmad2. (A-D) DAPI staining of wing imaginal discs from late third instar larvae of various TGFβ ligand mutants. Scale bar, 100µm. (E) Wing disc size of *myo* mutants are approximately 50% smaller than control w^{1118}, n=20 – 40. (F-I) Wing, leg, and haltere imaginal discs of $myo^{-/-}$ mutants are 50% smaller vs heterozygous controls $myo^{+/-}$. (H) size of different imaginal disc, normalized to controls. (I) Size ratio of haltere/wing disc (.25) or leg/wing disc (.3) is the same in *myo* mutants vs controls. (J-K) Phalloidin staining showing the apical actin-belt of epithelial cells in wing discs. Single confocal section is shown with the whole disc in insert. *myo* mutant discs cells are smaller vs control, area of 4 cells is plotted (L). Scale bar 10µm, n>25. M-N) Phospho-Histone H3-pSer10 (pH3) staining to mark mitotic cells in early third instar wing discs, showing no difference in number of mitotic cells in *myo* mutants. Number of mitotic cells in $100\mu m^2$ is plotted (O), scale bar 100 µm, n=5. (P-S) Phalloidin staining showing the late 3rd instar larvae skeletal muscle 6 and 7, muscle area (R) and number of nuclei (S) is plotted. Scale bar 100µm, n=10. *myo* mutants have 13% smaller muscles however the number of nuclei does not change. (T) Western blot analysis of phospho-dSmad2. *myo* mutants lack p-dSmad2 signal indicating loss of canonical signaling. (U) Model for canonical TGFβ signaling in wing imaginal disc via Myo/Babo/dSmad2. Characterization of specific Type-I Babo-isoform and Type-II receptor is demonstrated below. C-terminal activation of dSmad2 (yellow star) results in target gene regulation which is required for proper growth of imaginal discs.

Figure 2. Baboon-a regulates wing disc growth. (A) qPCR analysis of Babo isoform expression from late 3rd instar wing imaginal discs identifies only *babo-a* expression. *Rpl32* expression was used as housekeeping gene control. (B-I) Wings with isoform-specific knockdown of *babo*. RNAi for *Babo-a* throughout the wing imaginal disc (*esg-GAL4*) (C) or just the anterior compartment (*ci-GAL4*) (G) results in smaller adult wings and anterior compartment respectively. Scale bar 1mm. (J-K) Quantification of wing size and trichome density using *esg-GAL4* driver. *babo-a* RNAi wings are 40% smaller (J) however

the cells are larger (K). (L) Quantification of anterior compartment area and trichome density using *ci-GAL4*, *babo-a* RNAi strictly in the anterior domain shrinks the size by 50% accompanied by smaller cells densely packed (M). (N-O) RNAi for *babo-a* using *Hh-GAL4* is pupal lethal. Representative image of late larval imaginal discs of control (N) vs *babo-A* RNAi (O), with *UAS-GFP* used to mark expression domain of *Hh-GAL4*. Scale bar 50µm. (P) Quantification of posterior domain of larval imaginal discs from *Hh-GAL4* driven RNAi for *babo* isoforms. Loss of *babo-a* results in 35% smaller posterior domain as well as 29% decrease in epithelium thickness (Q).

Figure 3. Babo-a and Punt are required for non-canonical silencing of *brk*. In the background of *Brk-LacZ* reporter line random GFP+ (green) clones were induced by heat shock 48 hours prior to analysis (see methods for details). GFP+ marked clones also express RNAi for the indicated genes to the left of respective panel. Clones at the lateral edges of the disc were analyzed for patterning defects of the *brk* reporter. (A-D) Analysis of Babo isoforms. (E-I) Analysis of Type-II receptor. (A-I) Maximum intensity projections of wing imaginal discs stained with DAPI (blue) and anti β-gal (red), and fluorescent clone marker (green), scale bar = 100µm. (A'-I') Single confocal section of higher magnification of insert in (A-I) showing GFP+ marked clone expressing RNAi for indicated genes. Clones are outlined with white line, scale bar = 25µm. (A''-I'') Same confocal section as in (A'-I') with outlined clones showing *brk-LacZ* reporter expression pattern, scale bar = 25µm. *Brk* reporter is ectopically silenced in dSmad2 RNAi clones (A and E). This ectopic silencing is rescued by the concomitant RNAi of Babo-a alone (A'' vs B'') but not Babo-b or Babo-c (A'' vs C'' or D''). Similarly the dSmad2 RNAi dependent *brk* reporter silencing (E'') can be rescued by the concomitant RNAi of Type-II receptor Punt (E'' vs G'') but not Wit (E'' vs F''). For a control RNAi for *punt*, plus *wit* appears different than in the *brk* reporter patterning compared to RNAi for *wit* alone (F'' vs H''). As a further specificity test we ensured that the dSmad2 RNAi dependent silencing of the *brk* reporter is not mediated by Dpp-Tkv activation. RNAi for

Thickveins (BMP Type-I receptor) does not rescue ectopic *brk* silencing (E'' vs I''), indicating the loss of dSmad2 leads to *brk* silencing in lateral clones due to ectopic signaling by the TGFβ/Activin branch.

Figure 4. Muscle derived Myo is required for non-canonical Babo activity in imaginal discs. (A) 3rd instar larval fillet showing *myo-GAL4* driving CD8-GFP (green), DAPI (blue) counterstain to image all tissues in the field of view. DAPI channel (A') shows muscle and cuticle-associated cell nuclei, as well as the brain and several imaginal discs. GFP channel (A'') represents the expression pattern of the *myo-GAL4* reporter transgene. Note that the wing imaginal discs does not express detectable GFP, scale bar = 500 µm. (B) Higher magnification of 3rd instar larval brain from *myo>NLS-GFP* showing expression in glial cells, scale bar = 100 µm. (C-E) *myo* is epistatic to *dSmad2*, and rescues the disc overgrowth phenotype. *dSmad2f4* mutant discs (C) are overgrown, however *myo* mutant discs (D) retain the normal shape of the tissue. The *dSmad2f4;;;myo* double mutant discs (E) are similar to *myo* mutant discs, demonstrating rescue of the overgrowth phenotype, and that Myo can function in non-canonical Babo activation. (F-K) Muscle specific RNAi of *myo* is sufficient to rescue wing disc overgrowth phenotype of *dSmad2* mutants. RNAi of *myo* ubiquitously using *da-GAL4* rescues the wing disc overgrowth (F vs G), phenocopying double *dSmad2;;;myo* double mutants (E vs G). RNAi of *myo* in either wing discs (*esg-GAL4*) or glia (*repo-GAL4*) is unable to rescue disc overgrowth (F vs H or I). RNAi of *myo* in larval muscles using *Mef2-GAL4* or *MHC-GAL4* rescues the disc overgrowth phenotype (F vs J or K), which phenocopies ubiquitous *myo* RNAi (G vs J or K). C-K, scale bar = 100µm

Figure 5. Overexpression of *myo* in muscles and fat-body rescues wing disc size of *myo* mutants. (A-B) *Myo* mutant discs (B) are smaller than heterozygous controls (A). (C-E) wing discs from *myo* overexpression rescue experiments. *Myo* overexpression in glial cells using *Repo-GAL4* partially rescues wing disc size (B vs C). Overexpression in muscles completely rescues *myo* mutant discs back to wild

type size (B vs D vs A). *Myo* is not normally expressed in the fat-body (Fig 4). However, ectopic overexpression in the fat-body is sufficient to rescue discs back to wild-type size (B vs E vs A). (F) Quantification of wing discs size from (A-E). scale bar = 100 µm

Figure S1. *myo* mutants show no defects in cell death or cell growth. (A-B) Late 3rd instar larval wing discs stained for cleaved-caspase 3 shows no increase in cell death of *myo* mutant discs. (C-D) Early 3rd instar larval wing discs stained for phospho-S6, downstream of TOR signaling, reveals normal wild type patchy pattern in both *myo* and control discs. Scale bar 100 µm, n=5-10.

Figure S2. qPCR analysis of Babo isoform expression in various tissues from late 3rd instar larvae. Fat-body and gut express only Babo-c, whereas brains samples predominantly express Babo-a. The carcass sample produces detectable amounts of all three isoforms. This sample contains muscle, cuticle, and associated cells, precluding assignment of isoform expression to cell types. Expression levels are relative to *Rpl23*.

Figure S3. RNAi for *Babo-a* rescues wing disc overgrowth due to *dSmad2* RNAi. (A) Representative image of wild-type (control) imaginal disc. The width/height ratio is generally 0.9 (black line in D) for controls. (B) RNAi for *dSmad2* throughout the disc using *esg-GAL4* leads to ectopic *brk* silencing which results in overgrowth of the tissue along the anterior/posterior axis (widening) (red squares in D). (C) Simultaneous RNAi for *dSmad2* and *babo* (all isoforms) rescues the widening phenotype where the W/H ratio is back to 0.9 (purple triangles in D). (D) Quantification of pouch size from Babo isoform specific rescue experiments. Control samples (Blue diamonds) have an average ratio of 0.9; RNAi for *dSmad2* (red squares) leads to widening with a ratio of 0.6; RNAi for *babo* (all isoforms, purple triangles) or *babo-a* (green circles) alone rescues the widening back to wild type ratios. These discs are smaller than

wild type due to loss of canonical Baboon activity (Fig.1 and Fig.2). There is no effect to widening by knocking down either *babo-b* or *babo-c* (blue and yellow circles vs red squares).

Figure S4. *Plum* is required for non-canonical babo activity. *dSmad2$_{f4}$* null mutant wing discs are overgrown and show a widening phenotype. (A) *esg-GAL4* driving RNAi for *plum* in *dSmad2* mutant background, larvae raised at 18 °C suppresses the RNAi effect, and phenocopies *dSmad2* mutant discs which are overgrown. (B) *esg-GAL4* driving RNAi for *plum* in *dSmad2* mutant background, larvae raised at at 25 °C results in high RNAi expression which rescues the overgrowth phenotype. Scale bar = 200 μm.

Figure S5. (A) Muscle specific *myo* overexpression in addition to endogenous levels increases final wing size of adults. (B) Representative wings from A of controls (smaller wing) vs *MHC>myo* (larger wing). Wings are superimposed on top of each other to show difference in size.

Materials and Methods

Fly strains:

TGFβ mutants: *Myo1*, Act80, daw11, *dSmad2F4* are described previously (Awasaki et al., 2011; Peterson and O'Connor, 2013; Serpe and O'Connor, 2006; Zhu et al., 2008). Babo isoform RNAi lines and *myo-GAL4* are described previously (Awasaki et al., 2011). RNAi lines for *dSmad2* and *tkv* and the strategy used to generate new RNAi lines are described previously (Peterson and O'Connor, 2013; Peterson et al., 2012). New RNAi lines for *wit* targeted (1103-1608 of NM_079953.3), and *punt* targeted (1069-1582 of NM_169591.1). RNAi lines for *myo* targeted (2259-3503 of NM_166788.2) utilizing the "snapback" gDNA/cDNA hybrid method (Kalidas and Smith, 2002). Stocks and methods used for induction of GAL4 flp-out clones are described previously (Peterson and O'Connor, 2013). Briefly, clones were induced by incubation at 37°C for 30 minutes. Larvae were dissected 48 hours later at wandering L3 stage.

Ci-GAL4 and *hh-GAL4* were kind gifts from H. Steller (Rockefeller University). A version of MHC we labeled *MHCf-GAL4* was a kind gift from N. Perrimon (HHMI, Harvard). *UAS-plum-RNAi* was a gift from O. Schuldiner (Weizmann institute of sciences, Israel)

The following stocks are available from Bloomington *Drosophila* Stock Center: *da-GAL4* (#5460), *esg-GAL4* (#26816), *repo-GAL4* (#7415), *mef2-GAL4* (#27390), *MHC-GAL4* (#55133), cg-GAL4 (#7011), *UAS-mCD8::GFP*, *UAS-GFP.nls*,

Microscopy and Antibodies:

Cleaved Caspase-3 (Cell Signaling #9661), phospho-Histone3 (S10) (Sigma, H0412). For B14-LacZ reporter detection, wing discs were stained with anti-βgalactosidase (Promega, #Z378A). AlexaFluor 568 or 647 (Invitrogen) conjugated secondary antibodies were used when required.

Larval muscle and wing disc epithelium actin-belt were stained with rhodamine-phalloidin. To measure wing disc size, tissues were stained with DAPI.

Tissues for fluorescence microscopy were mounted with 80% Glycerol in PBS (0.1% TritonX-100). Wide-field images taken with a 20X objective on a Zeiss Axiovert microscope. CARV Confocal images were captured using a 20X objective on a Zeiss Axiovert. We also used the Zeiss LSM710 for confocal and "tile-scanning" imaging.

For adult wings, animals were dissected in 95% ethanol, and mounted with (50:50) Canadian balsam and wintergreen oil solution. Images were taken with a 4X objective (for whole wing) and 40X objective (for trichome density).

Images were processed in FIJI (imageJ). Wing disc size were calculated with the DAPI staining then using the threshold and measure functions. For larval muscle size and adult wing size, outlines were drawn using the polygon tool.

Western Blot:

Mid-late third instar larvae were dissected in cold PBS, and wing imaginal discs were collected and washed on ice. Total protein was extracted with RIPA buffer (Cell Signaling) with cOmplete protease inhibitor (Roche) and PhosSTOP phosphatase inhibitor (Roche). Lysates were mixed with reducing sample buffer, boiled, and 10 µl of sample were run on 4-12% graded precast gels (Invitrogen). Resolved protein samples were transferred to PVDF membrane. Membrane blocking and probing were performed using standard protocols for ECL. Antibodies used for western blot: phospho-Smad2 (Cell Signaling #3108), Tubulin (Sigma #T9026), goat anti-mouse HRP, and goat anti-rabbit HRP.

qPCR:

Late-third instar larvae were dissected in cold PBS, and tissues were pooled and washed in PBS on ice. Tissues were homogenized in Trizol (Invitrogen) and Total RNA purified using RNeasy Mini Kit (Qiagen). cDNA libraries were made using SuperScript-III (Invitrogen). qPCR was performed using SYBR green reagent (Roche) on a LightCycler 480. *Rpl23* was used as a housekeeping gene for normalization. We confirmed that primer sets for all three isoforms amplify equivalently using Babo-A, B and C control cDNA templates. The following qPCR primers were used for *babo* isoforms:

babo-a: F 5' GGCTTTTGTTTCACGTCCGTGGA 3'

babo-a: R 5' CTGTTTCAAATATCCTCTTCATAATCTCAT 3'

babo-b: F 5' GCAAGGACAGGGACTTCTG 3'

babo-b: R 5' GGCACATAATCTTGGACGGAG 3'

babo-c: F 5' GACCAGTTGCCACCTGAAGA 3'

babo-c: R 5' TGGCACATAATCTGGTAGGACA 3'

Statistics:

Statistical analysis were performed using Prism 6 (Graphpad) software. All experiments were repeated at least twice. Sample size was determined using published methods in the field. Data collection and analysis were not blind. Quantitative data are plotted as mean with standard deviations. Significance were determined using 2-tailed t-test with Welch's correction or an ANOVA with multiple comparisons. P values < 0.05 = *, < 0.01 = **, < 0.001 = ***.

Competing interest

The authors declare no competing or financial interests

Acknowledgements

We would like to thank: MaryJane O'Connor, and Heidi Bretscher, Tom Neufeld, Jeff Simon, and Jim Ervasti for comments on the manuscript. Bloomington Drosophila Stock Center for numerous fly lines. *Ci-GAL4* and *hh-GAL4* lines were a gift from Herman Steller

Author Contribution

Conceptualization: A.U., A.J.P, and M.B.O.; experimentation and data analysis: A.U. and A.J.P (fig 4, C-E); writing: A.U., A.J.P. and M.B.O.

Funding

National Institute of Health grant 1R35GM118029

References

Akiyama, T., Marqués, G. and Wharton, K. A. (2012). A large bioactive BMP ligand with distinct signaling properties is produced by alternative proconvertase processing. *Sci. Signal.* **5**, ra28.

Augustin, H., McGourty, K., Steinert, J. R., Cochemé, H. M., Adcott, J., Cabecinha, M., Vincent, A., Halff, E. F., Kittler, J. T., Boucrot, E., et al. (2017). Myostatin-like proteins regulate synaptic function and neuronal morphology. *Development* **144**, 2445–2455.

Awasaki, T., Huang, Y., O'Connor, M. B. and Lee, T. (2011). Glia instruct developmental neuronal remodeling through TGF-β signaling. *Nat. Neurosci.* **14**, 821–3.

Boulan, L., Milán, M. and Léopold, P. (2015). The Systemic Control of Growth. *Cold Spring Harb. Perspect. Biol.* **7**,.

Brummel, T. J., Twombly, V., Marqués, G., Wrana, J. L., Newfeld, S. J., Attisano, L., Massagué, J., O'Connor, M. B. and Gelbart, W. M. (1994). Characterization and relationship of Dpp receptors encoded by the saxophone and thick veins genes in Drosophila. *Cell* **78**, 251–61.

Brummel, T., Abdollah, S., Haerry, T. E., Shimell, M. J., Merriam, J., Raftery, L., Wrana, J. L. and O'Connor, M. B. (1999). The Drosophila Activin receptor Baboon signals through dSmad2 and controls cell proliferation but not patterning during larval development. *Genes Dev.* **13**, 98–111.

Campbell, G. and Tomlinson, a (1999). Transducing the Dpp morphogen gradient in the wing of Drosophila: regulation of Dpp targets by brinker. *Cell* **96**, 553–62.

Childs, S. R., Wrana, J. L., Arora, K., Attisano, L., O'Connor, M. B. and Massagué, J. (1993). Identification of a Drosophila activin receptor. *Proc. Natl. Acad. Sci. U. S. A.* **90**, 9475–9.

Chng, W. A., Sleiman, M. S. B., Schüpfer, F. and Lemaitre, B. (2014). Transforming growth factor β/activin signaling functions as a sugar-sensing feedback loop to regulate digestive enzyme expression. *Cell Rep.* **9**, 336–348.

De Santis, C., Wade, N. M., Jerry, D. R., Preston, N. P., Glencross, B. D. and Sellars, M. J. (2011). Growing backwards: an inverted role for the shrimp ortholog of vertebrate myostatin and GDF11. *J. Exp. Biol.* **214**, 2671–2677.

Demontis, F., Patel, V. K., Swindell, W. R. and Perrimon, N. (2014). Intertissue control of the nucleolus via a myokine-dependent longevity pathway. *Cell Rep.* **7**, 1481–1494.

Di Cara, F. and King-Jones, K. (2016). The Circadian Clock Is a Key Driver of Steroid Hormone Production in Drosophila. *Curr. Biol.* **26**, 2469–2477.

Droujinine, I. A. and Perrimon, N. (2013). Defining the interorgan communication network: systemic coordination of organismal cellular processes under homeostasis and localized stress. *Front. Cell. Infect. Microbiol.* **3**, 82.

Dutta, D., Anant, S., Ruiz-Gomez, M., Bate, M. and VijayRaghavan, K. (2004). Founder myoblasts and fibre number during adult myogenesis in Drosophila. *Development* **131**, 3761–3772.

Egerman, M. A., Cadena, S. M., Gilbert, J. A., Meyer, A., Nelson, H. N., Swalley, S. E., Mallozzi, C., Jacobi, C., Jennings, L. L., Clay, I., et al. (2015). GDF11 Increases with Age and Inhibits Skeletal Muscle Regeneration. *Cell Metab.* **22**, 164–74.

El-Brolosy, M. A. and Stainier, D. Y. R. (2017). Genetic compensation: A phenomenon in search of mechanisms. *PLoS Genet.* **13**, e1006780.

El-Brolosy, M. A., Kontarakis, Z., Rossi, A., Kuenne, C., Günther, S., Fukuda, N., Kikhi, K., Boezio, G. L. M., Takacs, C. M., Lai, S.-L., et al. (2019). Genetic compensation triggered by mutant mRNA degradation. *Nature* **568**, 193–197.

Fuentes-Medel, Y., Ashley, J., Barria, R., Maloney, R., Freeman, M. and Budnik, V. (2012). Integration of a retrograde signal during synapse formation by glia-secreted TGF-beta ligand. *Curr Biol* **22**, 1831–1838.

Ghosh, A. C. and O'Connor, M. B. (2014). Systemic Activin signaling independently regulates sugar homeostasis, cellular metabolism, and pH balance in Drosophila melanogaster. *Proc. Natl. Acad. Sci. U. S. A.* **111**, 5729–34.

Gibbens, Y. Y., Warren, J. T., Gilbert, L. I. and O'Connor, M. B. (2011). Neuroendocrine regulation of Drosophila metamorphosis requires TGFbeta/Activin signaling. *Development* **138**, 2693–703.

Graveley, B. R., Brooks, A. N., Carlson, J. W., Duff, M. O., Landolin, J. M., Yang, L., Artieri, C. G., van Baren, M. J., Boley, N., Booth, B. W., et al. (2011). The developmental transcriptome of Drosophila melanogaster. *Nature* **471**, 473–9.

Grewal, S. S. (2012). Controlling animal growth and body size - does fruit fly physiology point the way? *F1000 Biol. Rep.* **4**, 12.

Grobet, L., Martin, L. J., Poncelet, D., Pirottin, D., Brouwers, B., Riquet, J., Schoeberlein, A., Dunner, S., Ménissier, F., Massabanda, J., et al. (1997). A deletion in the bovine myostatin gene causes the double-muscled phenotype in cattle. *Nat. Genet.* **17**, 71–4.

Gunage, R. D., Reichert, H. and VijayRaghavan, K. (2014). Identification of a new stem cell population that generates Drosophila flight muscles. *Elife* **3**,.

Haerry, T. E., Khalsa, O., O'Connor, M. B. and Wharton, K. a (1998). Synergistic signaling by two BMP ligands through the SAX and TKV receptors controls wing growth and patterning in Drosophila. *Development* **125**, 3977–87.

Hariharan, I. K. (2015). Organ Size Control: Lessons from Drosophila. *Dev. Cell* **34**, 255–65.

Heldin, C.-H. and Moustakas, A. (2016). Signaling Receptors for TGF-β Family Members. *Cold Spring Harb. Perspect. Biol.* **8**,.

Hevia, C. F. and de Celis, J. F. (2013). Activation and function of TGFβ signalling during Drosophila wing development and its interactions with the BMP pathway. *Dev. Biol.* **377**, 138–53.

Hevia, C. F., López-Varea, A., Esteban, N. and de Celis, J. F. (2017). A Search for Genes Mediating the Growth Promoting Function of TGFβ in the Drosophila melanogaster Wing Disc. *Genetics* **206**, genetics.116.197228.

Hinck, A. P., Mueller, T. D. and Springer, T. A. (2016). Structural Biology and Evolution of the TGF-β Family. *Cold Spring Harb. Perspect. Biol.* **8**,.

Jensen, P. A., Zheng, X., Lee, T. and O'Connor, M. B. (2009). The Drosophila Activin-like ligand Dawdle signals preferentially through one isoform of the Type-I receptor Baboon. *Mech. Dev.* **126**, 950–7.

Johnston, L. A. and Gallant, P. (2002). Control of growth and organ size in Drosophila. *Bioessays* **24**, 54–64.

Kalidas, S. and Smith, D. P. (2002). Novel genomic cDNA hybrids produce effective RNA interference in adult Drosophila. *Neuron* **33**, 177–84.

Lecuit, T., Brook, W., Ng, M., Calleja, M., Sun, H. and Cohen, S. (1996). Two distinct mechanisms for long-range patterning by Decapentaplegic in the Drosophila wing. *Nature* **381**, 387–393.

Lee-Hoeflich, S. T., Zhao, X., Mehra, A. and Attisano, L. (2005). The Drosophila type II receptor, Wishful thinking, binds BMP and myoglianin to activate multiple TGF?? family signaling pathways. *FEBS Lett.* **579**, 4615–4621.

Lee, J. Y., Hopkinson, N. S. and Kemp, P. R. (2011). Myostatin induces autophagy in skeletal muscle in vitro. *Biochem. Biophys. Res. Commun.* **415**, 632–6.

Letsou, A., Arora, K., Wrana, J. L., Simin, K., Twombly, V., Jamal, J., Staehling-Hampton, K., Hoffmann, F. M., Gelbart, W. M. and Massagué, J. (1995). Drosophila Dpp signaling is mediated by the punt gene product: a dual ligand-binding type II receptor of the TGF beta receptor family. *Cell* **80**, 899–908.

Lo, P. C. and Frasch, M. (1999). Sequence and expression of myoglianin, a novel Drosophila gene of the TGF-beta superfamily. *Mech. Dev.* **86**, 171–5.

Marqués, G., Bao, H., Haerry, T. E., Shimell, M. J., Duchek, P., Zhang, B. and O'Connor, M. B. (2002). The Drosophila BMP type II receptor Wishful Thinking regulates neuromuscular synapse morphology and function. *Neuron* **33**, 529–43.

Martin, F. A., Herrera, S. C. and Morata, G. (2009). Cell competition, growth and size control in the Drosophila wing imaginal disc. *Development* **136**, 3747–3756.

McPherron, A. C. and Lee, S. J. (1997). Double muscling in cattle due to mutations in the myostatin gene. *Proc. Natl. Acad. Sci. U. S. A.* **94**, 12457–61.

McPherron, A. C., Huynh, T. V and Lee, S.-J. (2009). Redundancy of myostatin and growth/differentiation factor 11 function. *BMC Dev. Biol.* **9**, 24.

Minami, M., Kinoshita, N., Kamoshida, Y., Tanimoto, H. and Tabata, T. (1999). brinker is a target of Dpp in Drosophila that negatively regulates Dpp-dependent genes. *Nature* **398**, 242–6.

Mirth, C. K. and Shingleton, A. W. (2012). Integrating body and organ size in Drosophila: Recent advances and outstanding problems. *Front. Endocrinol. (Lausanne).* **3**, 1–13.

Morikawa, M., Derynck, R. and Miyazono, K. (2016). TGF-β and the TGF-β Family: Context-Dependent Roles in Cell and Tissue Physiology. *Cold Spring Harb. Perspect. Biol.* **8**, a021873.

Moss-Taylor, L., Upadhyay, A., Pan, X., Kim, M.-J. and O'Connor, M. B. (2019). Motoneuron-derived Activinβ regulates Drosophila body size and tissue-scaling during larval growth and adult development. *bioRxiv* 661363.

Müller, B., Hartmann, B., Pyrowolakis, G., Affolter, M. and Basler, K. (2003). Conversion of an extracellular Dpp/BMP morphogen gradient into an inverse transcriptional gradient. *Cell* **113**, 221–33.

Nijhout, H. F. (2003). The control of body size in insects. *Dev. Biol.* **261**, 1–9.

Parker, L., Ellis, J. E., Nguyen, M. Q. and Arora, K. (2006). The divergent TGF-β ligand Dawdle utilizes an activin pathway to influence axon guidance in Drosophila. *Development* **133**, 4981–4991.

Peterson, A. J. and O'Connor, M. B. (2013). Activin receptor inhibition by Smad2 regulates Drosophila wing disc patterning through BMP-response elements. *Development* **140**, 649–59.

Peterson, A. J. and O'Connor, M. B. (2014). Strategies for exploring TGF-β signaling in Drosophila.

Methods **68**, 183–93.

Peterson, A. J., Jensen, P. A., Shimell, M., Stefancsik, R., Wijayatonge, R., Herder, R., Raftery, L. A. and O'Connor, M. B. (2012). R-Smad competition controls activin receptor output in Drosophila. *PLoS One* **7**, e36548.

Restrepo, S., Zartman, J. J. and Basler, K. (2014). Coordination of patterning and growth by the morphogen DPP. *Curr. Biol.* **24**, R245–R255.

Rodriguez, J., Vernus, B., Chelh, I., Cassar-Malek, I., Gabillard, J. C., Hadj Sassi, A., Seiliez, I., Picard, B. and Bonnieu, A. (2014). Myostatin and the skeletal muscle atrophy and hypertrophy signaling pathways. *Cell. Mol. Life Sci.* **71**, 4361–71.

Romero-Pozuelo, J., Demetriades, C., Schroeder, P. and Teleman, A. A. (2017). CycD/Cdk4 and Discontinuities in Dpp Signaling Activate TORC1 in the Drosophila Wing Disc. *Dev. Cell* **42**, 376-387.e5.

Sander, V., Eivers, E., Choi, R. H. and De Robertis, E. M. (2010). Drosophila Smad2 opposes Mad signaling during wing vein development. *PLoS One* **5**, e10383.

Serpe, M. and O'Connor, M. B. (2006). The metalloprotease tolloid-related and its TGF-beta-like substrate Dawdle regulate Drosophila motoneuron axon guidance. *Development* **133**, 4969–79.

Setiawan, L., Pan, X., Woods, A. L., O'Connor, M. B. and Hariharan, I. K. (2018). The BMP2/4 ortholog Dpp can function as an inter-organ signal that regulates developmental timing. *Life Sci. alliance* **1**, e201800216.

Shimmi, O. and O'Connor, M. B. (2003). Physical properties of Tld, Sog, Tsg and Dpp protein interactions are predicted to help create a sharp boundary in Bmp signals during dorsoventral patterning of the Drosophila embryo. *Development* **130**, 4673–82.

Shingleton, A. W., Frankino, W. A., Flatt, T., Nijhout, H. F. and Emlen, D. J. (2007). Size and shape: the developmental regulation of static allometry in insects. *Bioessays* **29**, 536–48.

Shingleton, A. W., Mirth, C. K. and Bates, P. W. (2008). Developmental model of static allometry in holometabolous insects. *Proc. R. Soc. B Biol. Sci.* **275**, 1875–1885.

Sinha, M., Jang, Y. C., Oh, J., Khong, D., Wu, E. Y., Manohar, R., Miller, C., Regalado, S. G., Loffredo, F. S., Pancoast, J. R., et al. (2014). Restoring Systemic GDF11 Levels Reverses Age-Related Dysfunction in Mouse Skeletal Muscle. *Science (80-.).* **344**, 649–652.

Song, W., Owusu-Ansah, E., Hu, Y., Cheng, D., Ni, X., Zirin, J. and Perrimon, N. (2017). Activin signaling mediates muscle-to-adipose communication in a mitochondria dysfunction-associated obesity model. *Proc. Natl. Acad. Sci.* **114**, 8596–8601.

Sopko, R. and Perrimon, N. (2013). Receptor Tyrosine Kinases in Drosophila Development. *Cold Spring Harb. Perspect. Biol.* **5**, a009050–a009050.

Teleman, A. A. (2009). Molecular mechanisms of metabolic regulation by insulin in Drosophila. *Biochem. J.* **425**, 13–26.

Trendelenburg, A. U., Meyer, A., Rohner, D., Boyle, J., Hatakeyama, S. and Glass, D. J. (2009). Myostatin reduces Akt/TORC1/p70S6K signaling, inhibiting myoblast differentiation and myotube size. *Am. J. Physiol. Cell Physiol.* **296**, C1258-70.

Uhlén, M., Fagerberg, L., Hallström, B. M., Lindskog, C., Oksvold, P., Mardinoglu, A., Sivertsson, Å., Kampf, C., Sjöstedt, E., Asplund, A., et al. (2015). Tissue-based map of the human proteome.

Science (80-.). **347**, 1260419.

Upadhyay, A., Moss-Taylor, L., Kim, M., Ghosh, A. C. and O'Connor, M. B. (2017). TGF-β Family Signaling in Drosophila. *Cold Spring Harb. Perspect. Biol.* **9**,.

Van Bortle, K., Peterson, A. J., Takenaka, N., O'Connor, M. B. and Corces, V. G. (2015). CTCF-dependent co-localization of canonical Smad signaling factors at architectural protein binding sites in D. melanogaster. *Cell Cycle* **14**, 2677–87.

Wartlick, O., Mumcu, P., Kicheva, a, Bittig, T., Seum, C., Jülicher, F. and González-Gaitán, M. (2011). Dynamics of Dpp signaling and proliferation control. *Science* **331**, 1154–1159.

Wolfman, N. M., McPherron, A. C., Pappano, W. N., Davies, M. V, Song, K., Tomkinson, K. N., Wright, J. F., Zhao, L., Sebald, S. M., Greenspan, D. S., et al. (2003). Activation of latent myostatin by the BMP-1/tolloid family of metalloproteinases. *Proc. Natl. Acad. Sci. U. S. A.* **100**, 15842–6.

Yu, X. M., Gutman, I., Mosca, T. J., Iram, T., Ozkan, E., Garcia, K. C., Luo, L. and Schuldiner, O. (2013). Plum, an immunoglobulin superfamily protein, regulates axon pruning by facilitating TGF-β signaling. *Neuron* **78**, 456–68.

Zheng, X., Zugates, C. T., Lu, Z., Shi, L., Bai, J. and Lee, T. (2006). Baboon/dSmad2 TGF-beta signaling is required during late larval stage for development of adult-specific neurons. *EMBO J.* **25**, 615–27.

Zhu, C. C., Boone, J. Q., Jensen, P. A., Hanna, S., Podemski, L., Locke, J., Doe, C. Q. and O'Connor, M. B. (2008). Drosophila Activin- and the Activin-like product Dawdle function redundantly to regulate proliferation in the larval brain. *Development* **135**, 513–521.

Figure 1

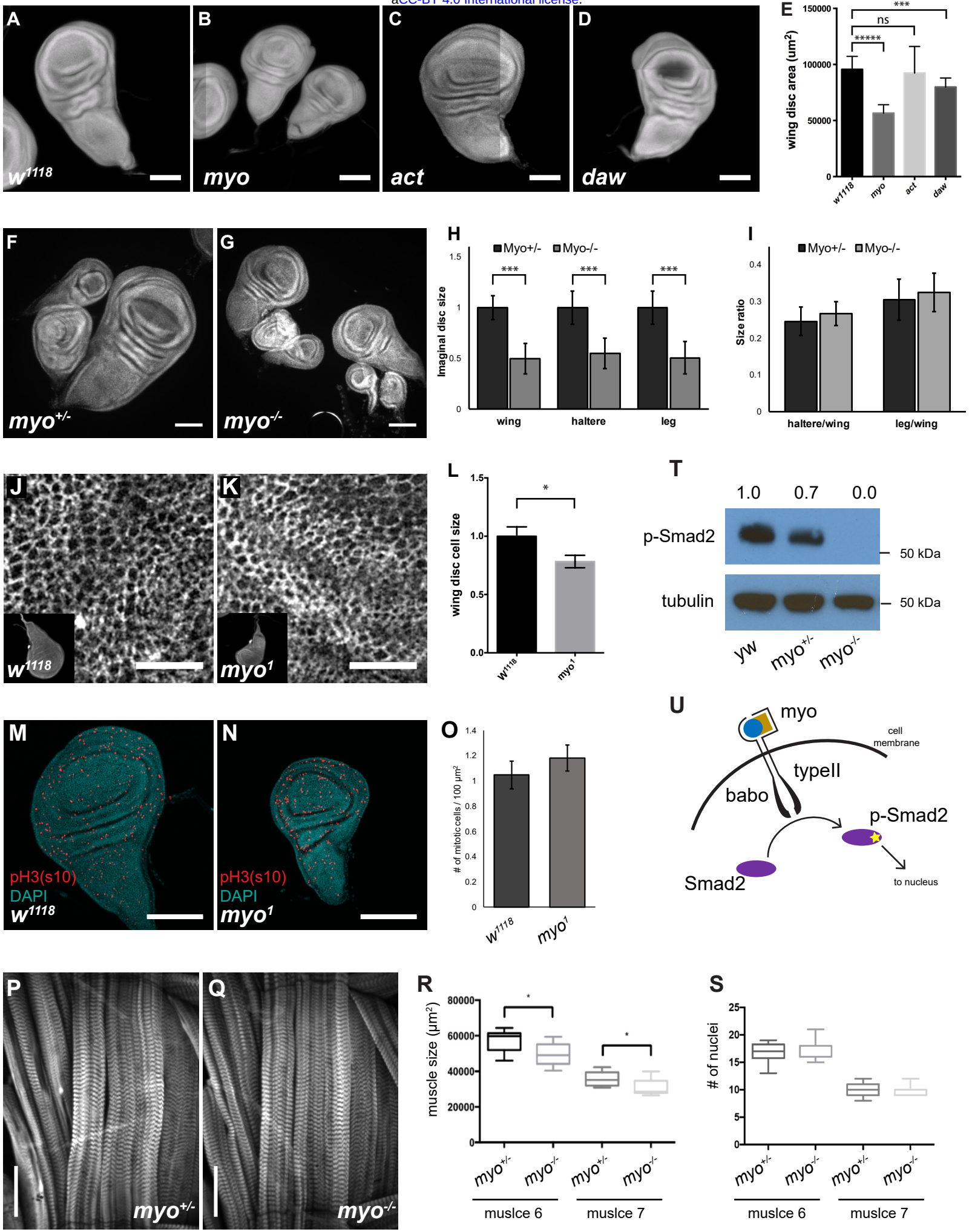

Figure 2

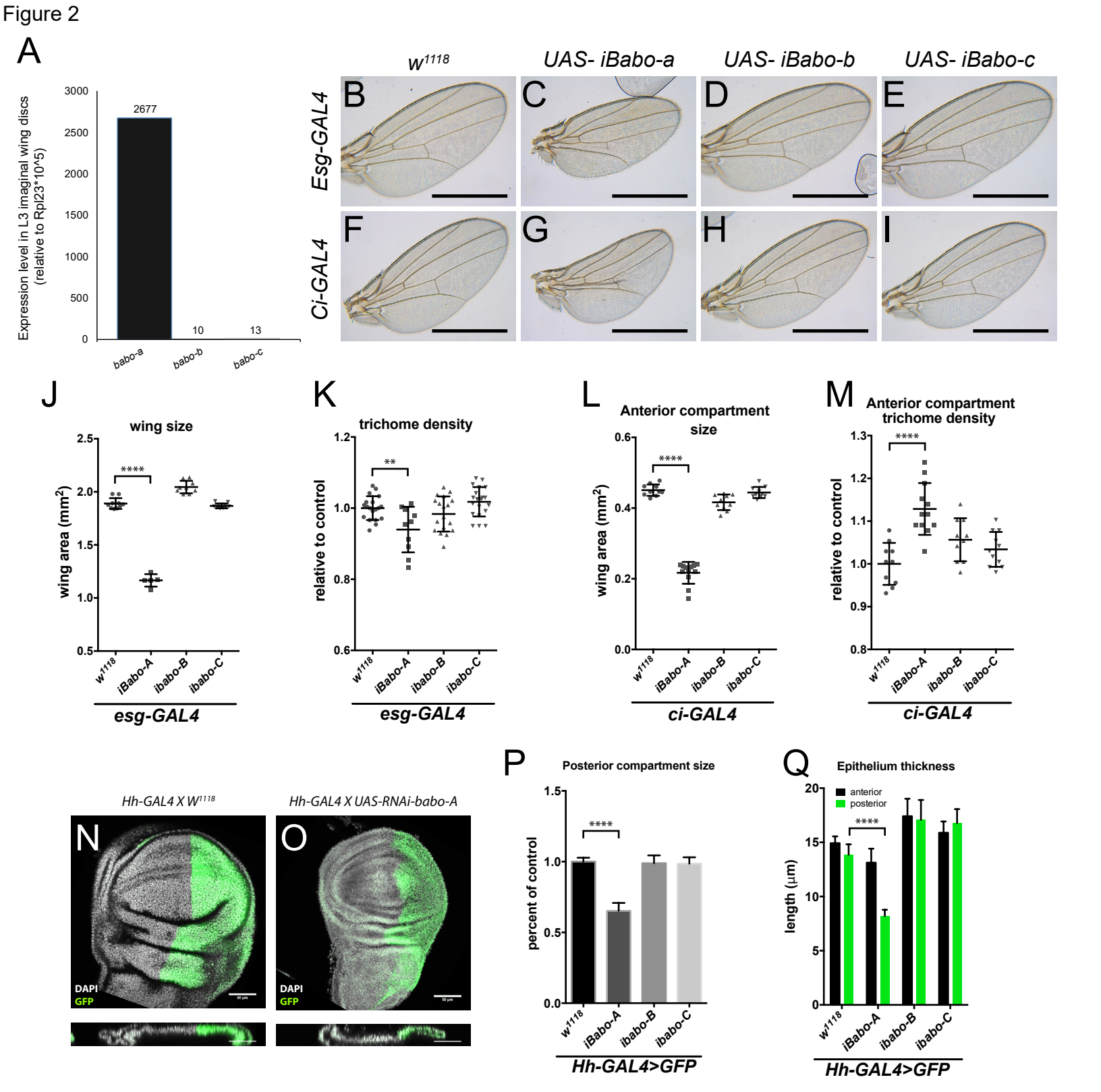
A
Expression level in L3 imaginal wing discs (relative to Rpl23*10^5)
3000
2500
2000
1500
1000
500
0
2677
10
13
babo-a
babo-b
babo-c
w1118
UAS- iBabo-a
UAS- iBabo-b
UAS- iBabo-c
Esg-GAL4
Ci-GAL4
B
C
D
E
F
G
H
I
J
wing size
wing area (mm2)
****
w1118
iBabo-A
ibabo-B
ibabo-C
esg-GAL4
K
trichome density
relative to control
**
esg-GAL4
L
Anterior compartment size
wing area (mm2)
****
ci-GAL4
M
Anterior compartment trichome density
relative to control
****
ci-GAL4
Hh-GAL4 X W1118
Hh-GAL4 X UAS-RNAi-babo-A
N
O
DAPI
GFP
P
Posterior compartment size
percent of control
****
Hh-GAL4>GFP
Q
Epithelium thickness
anterior
posterior
length (µm)
****
Hh-GAL4>GFP

Figure 3

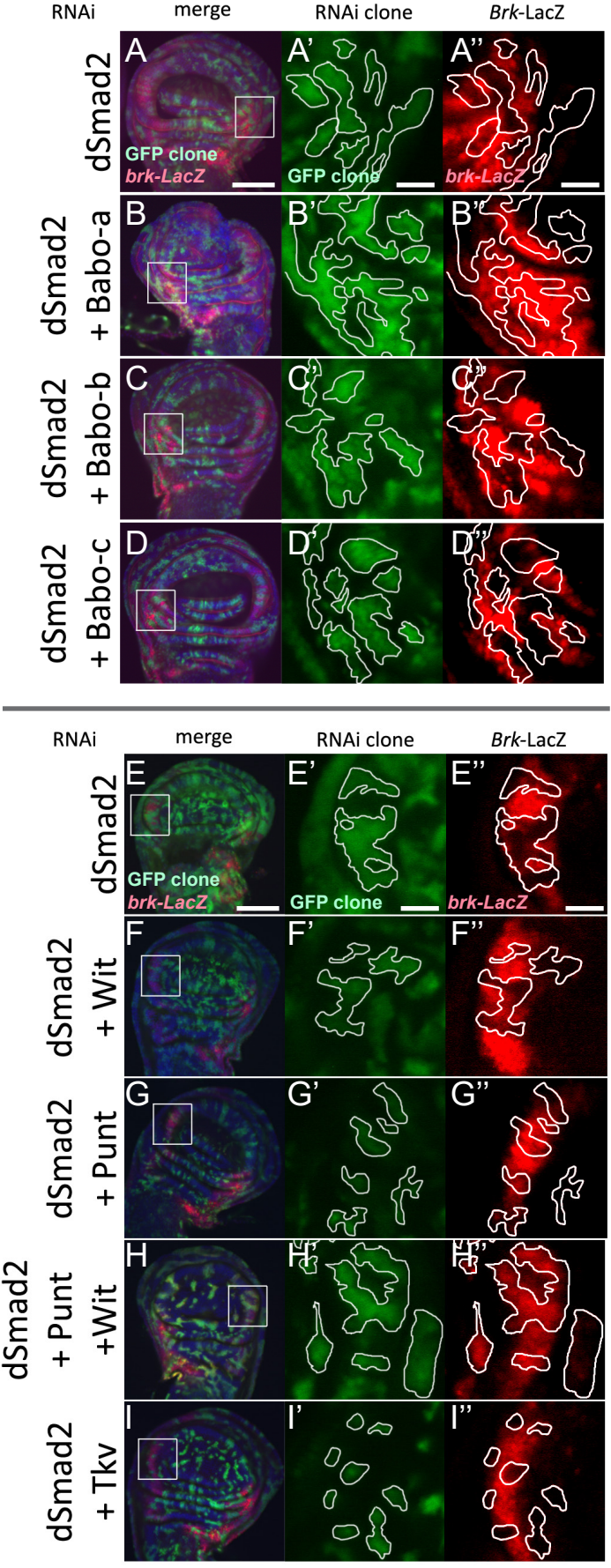
RNAi
merge
RNAi clone
Brk-LacZ
dSmad2
A
A'
A''
GFP clone
brk-LacZ
dSmad2 + Babo-a
B
B'
B''
dSmad2 + Babo-b
C
C'
C''
dSmad2 + Babo-c
D
D'
D''
dSmad2 + Punt +Wit
dSmad2 + Tkv
E
E'
E''
dSmad2 + Wit
F
F'
F''
dSmad2 + Punt
G
G'
G''
H
H'
H''
I
I'
I''

Figure 4

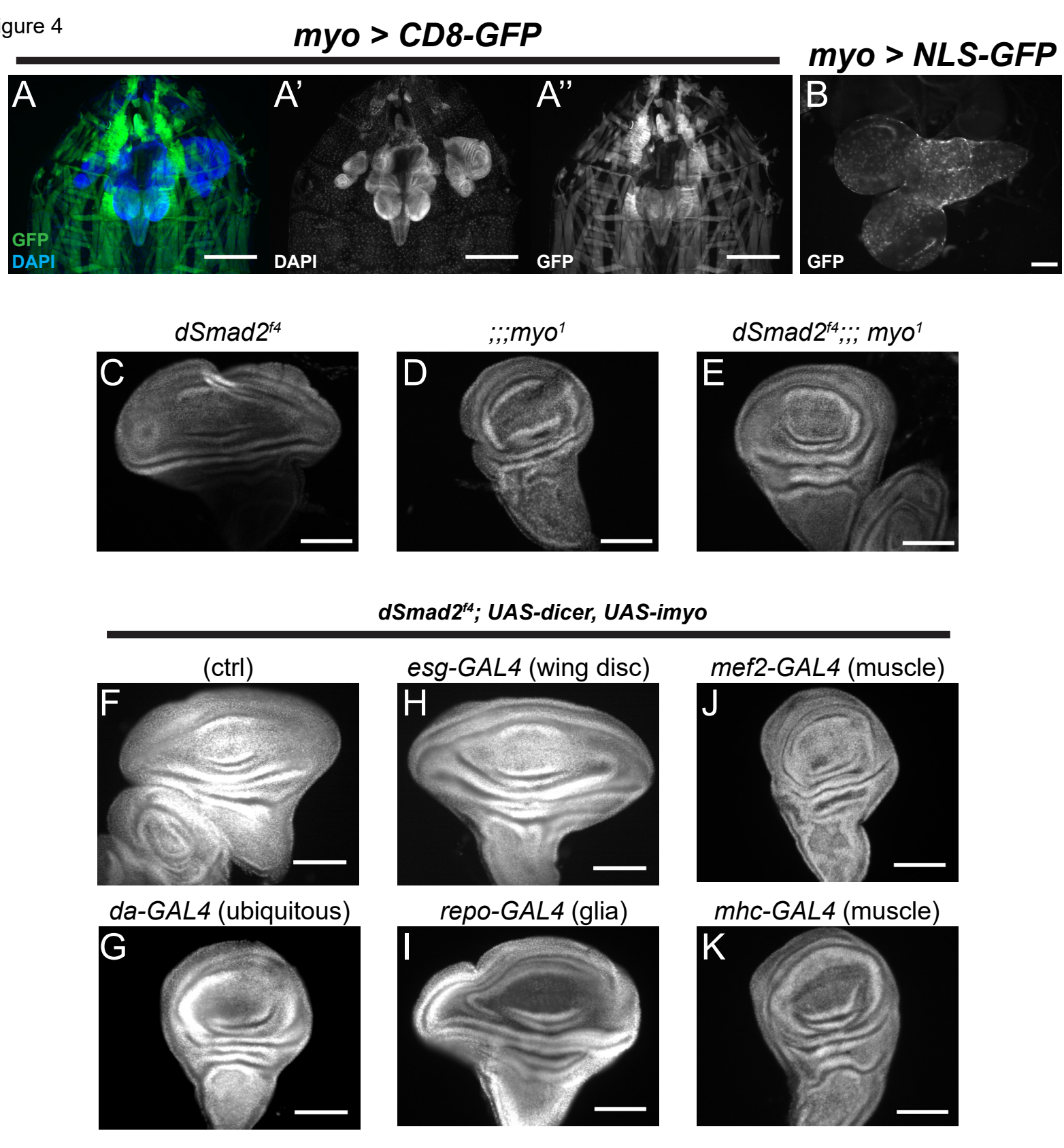
myo > CD8-GFP
myo > NLS-GFP
A
A'
A''
B
GFP
DAPI
DAPI
GFP
GFP
dSmad2f4
;;;myo1
dSmad2f4;;; myo1
C
D
E
dSmad2f4; UAS-dicer, UAS-imyo
(ctrl)
esg-GAL4 (wing disc)
mef2-GAL4 (muscle)
F
H
J
da-GAL4 (ubiquitous)
repo-GAL4 (glia)
mhc-GAL4 (muscle)
G
I
K

Figure 5

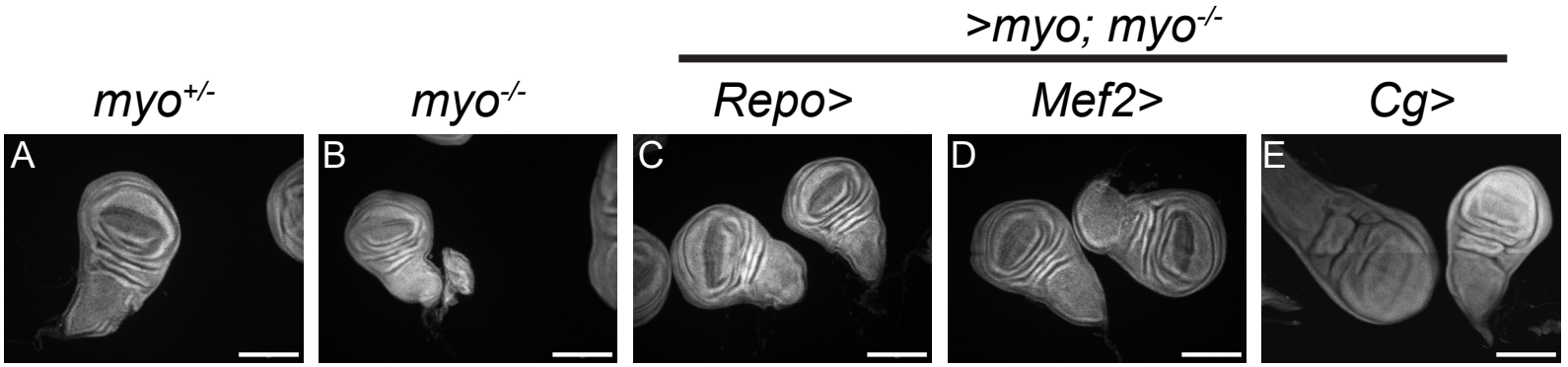
>myo; myo-/-
myo+/-
myo-/-
Repo>
Mef2>
Cg>
A
B
C
D
E

F

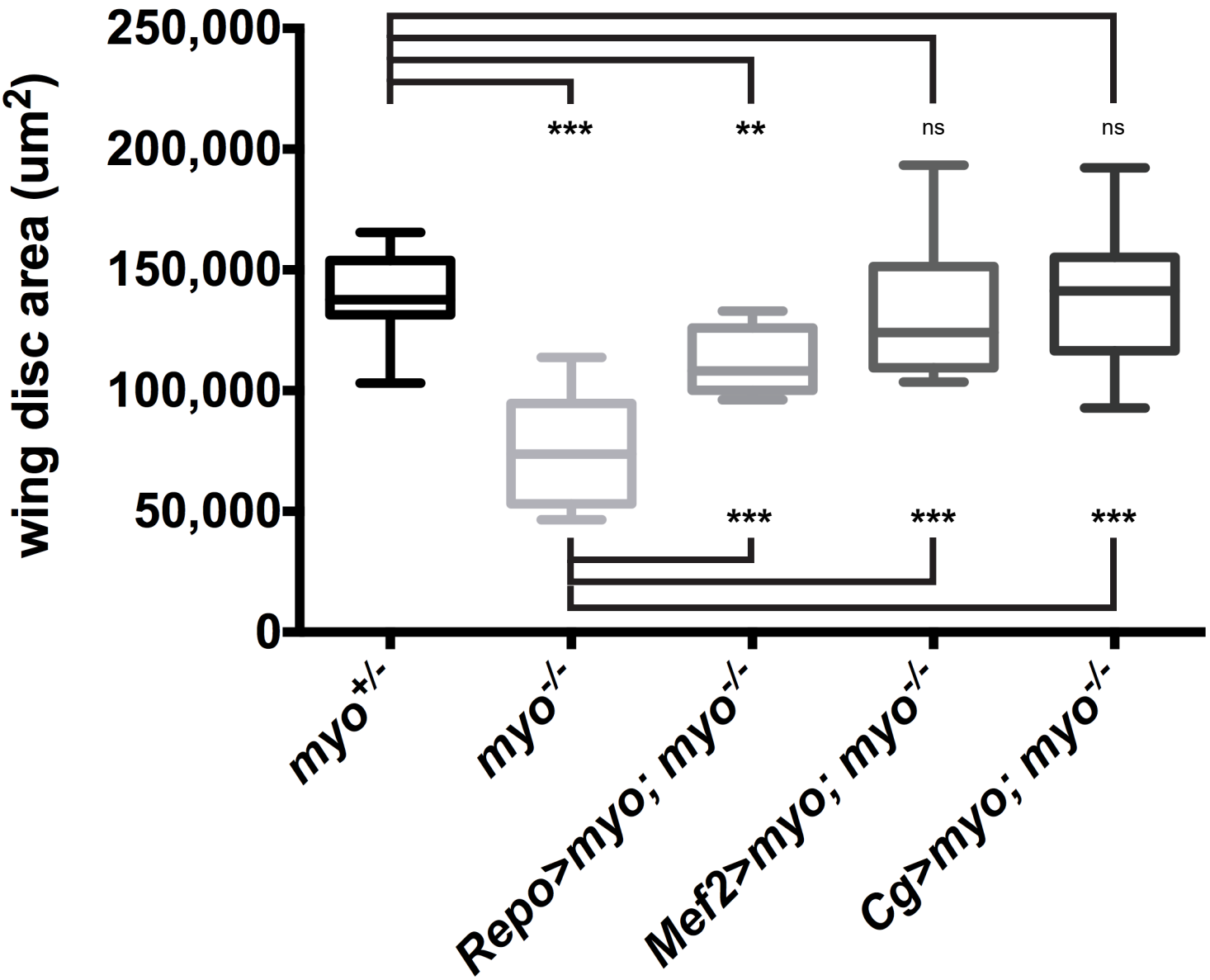
wing disc area (um2)
250,000
200,000
150,000
100,000
50,000
0
***
**
ns
ns
***
***
***
myo+/-
myo-/-
Repo>myo; myo-/-
Mef2>myo; myo-/-
Cg>myo; myo-/-

Figure S1

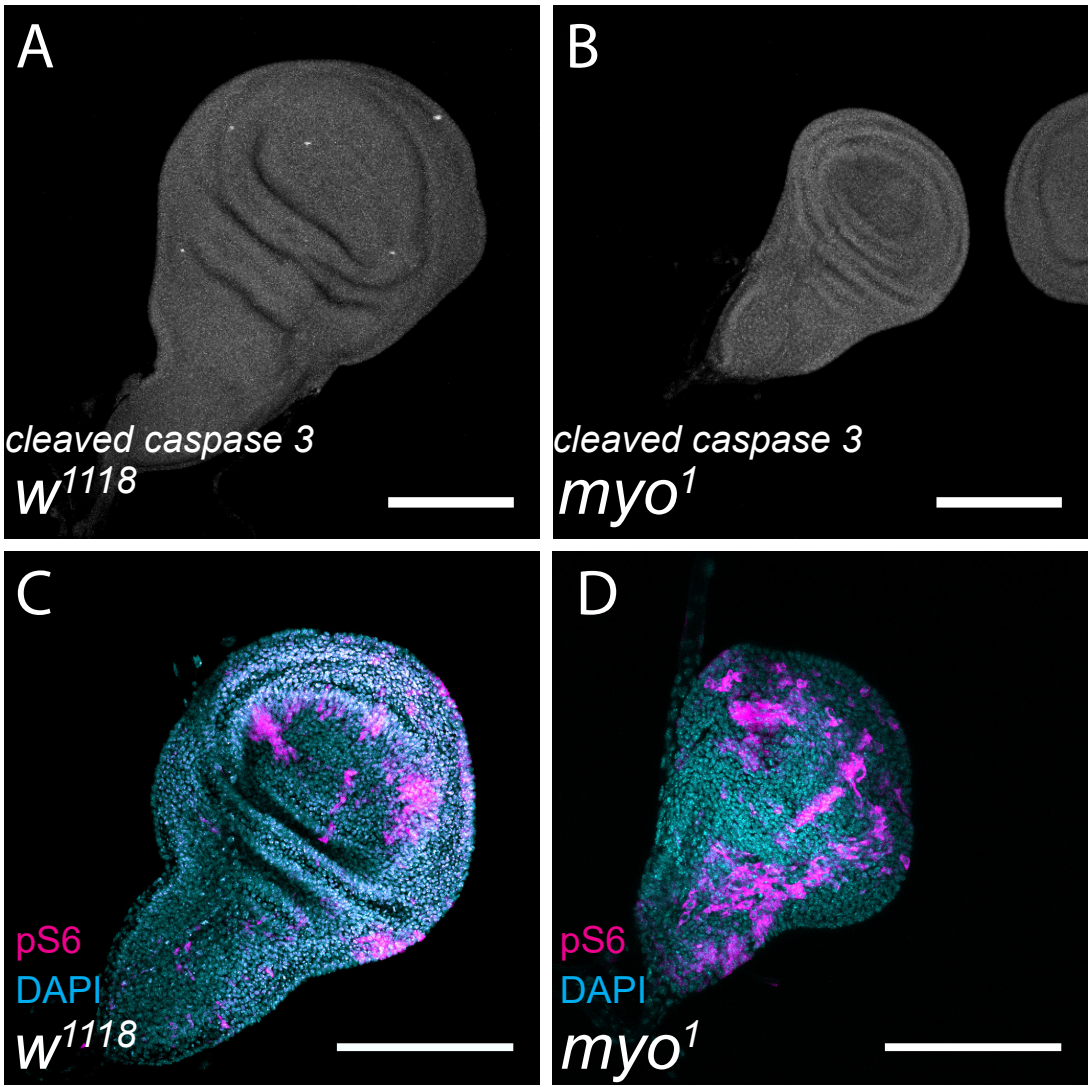
A
cleaved caspase 3
w1118
B
cleaved caspase 3
myo1
C
pS6
DAPI
w1118
D
pS6
DAPI
myo1

Figure S2

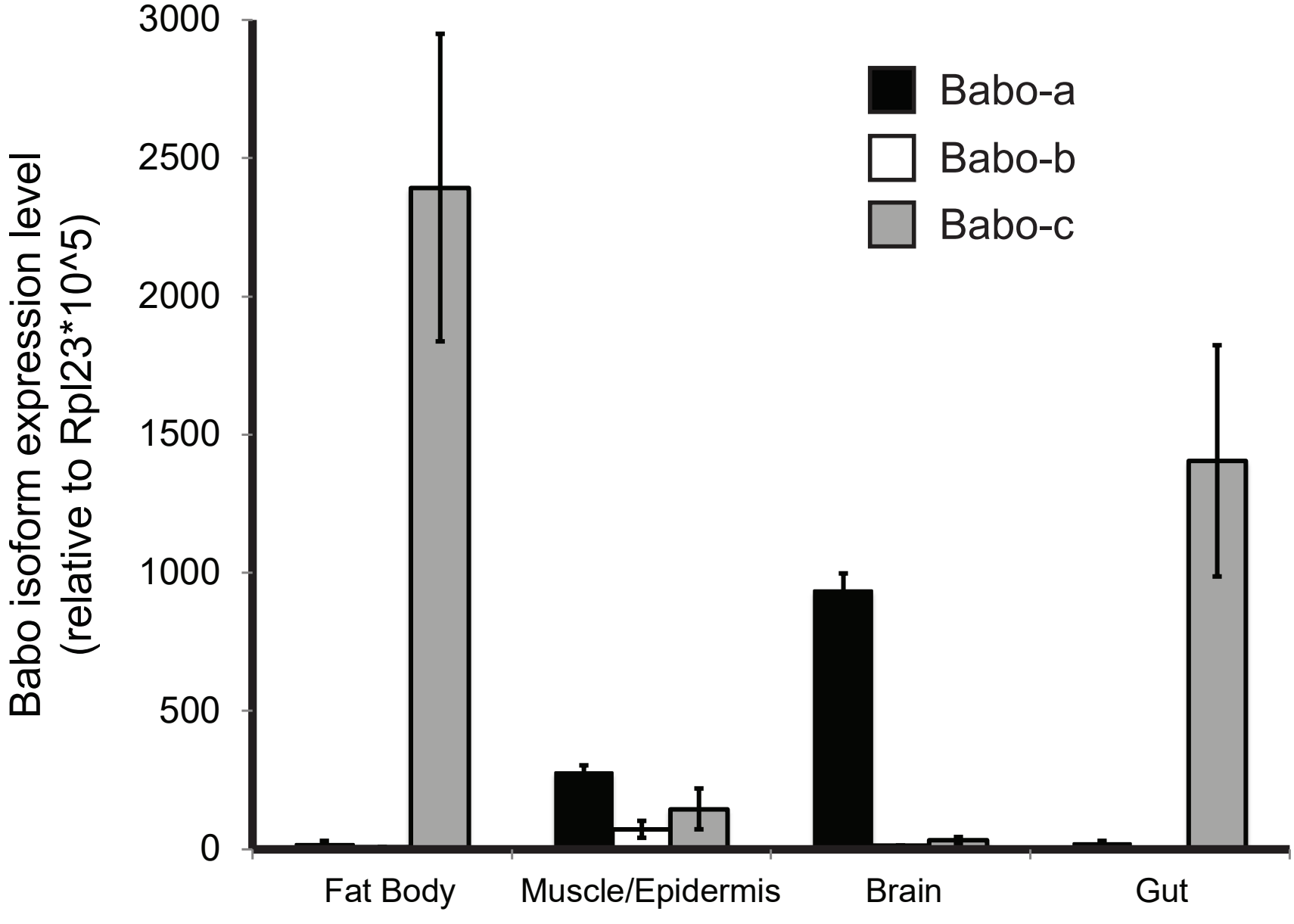
Babo isoform expression level
(relative to Rpl23*10^5)
3000
2500
2000
1500
1000
500
0
Babo-a
Babo-b
Babo-c
Fat Body
Muscle/Epidermis
Brain
Gut

Figure S3

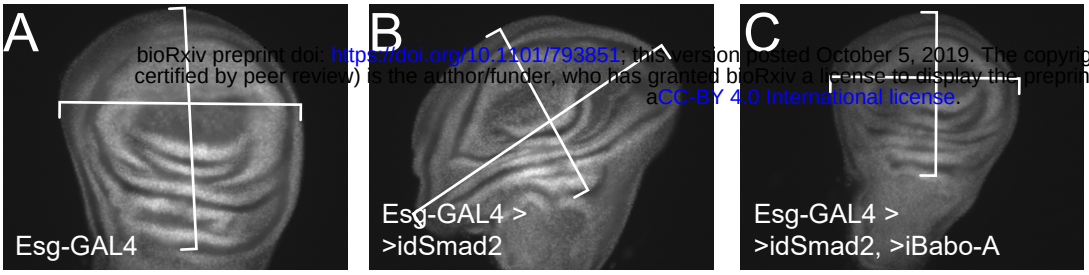

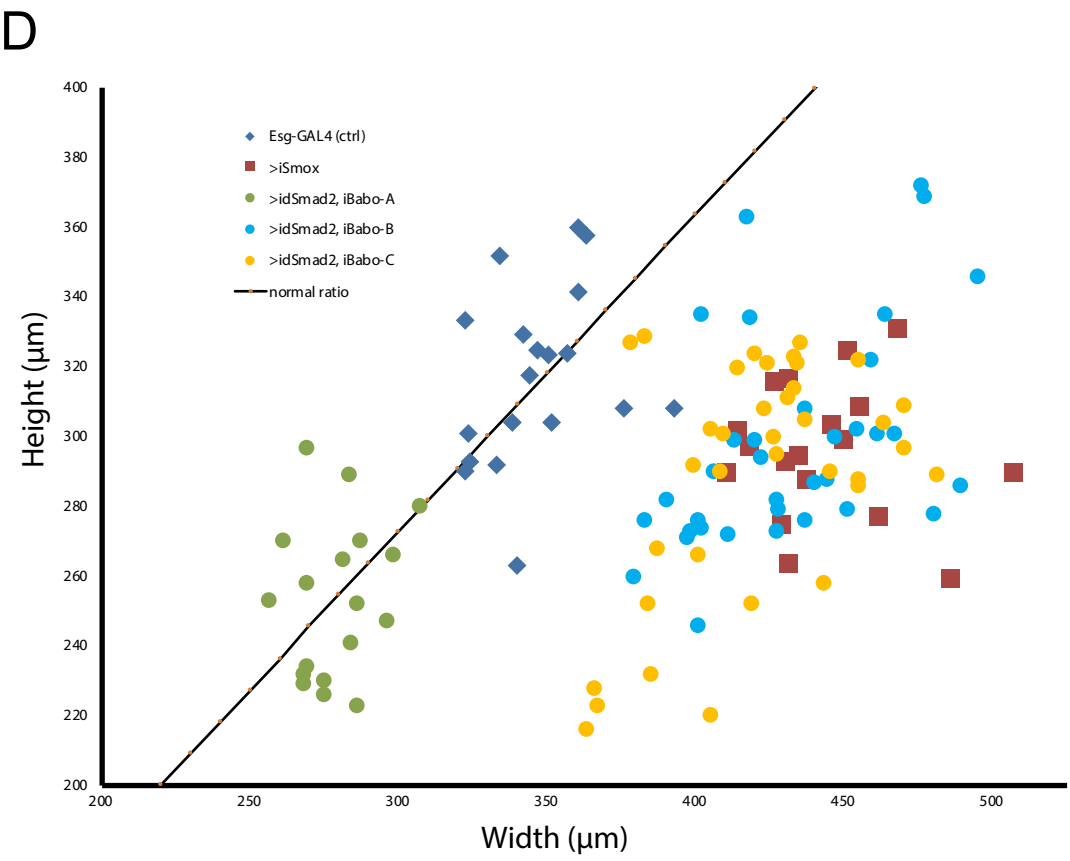

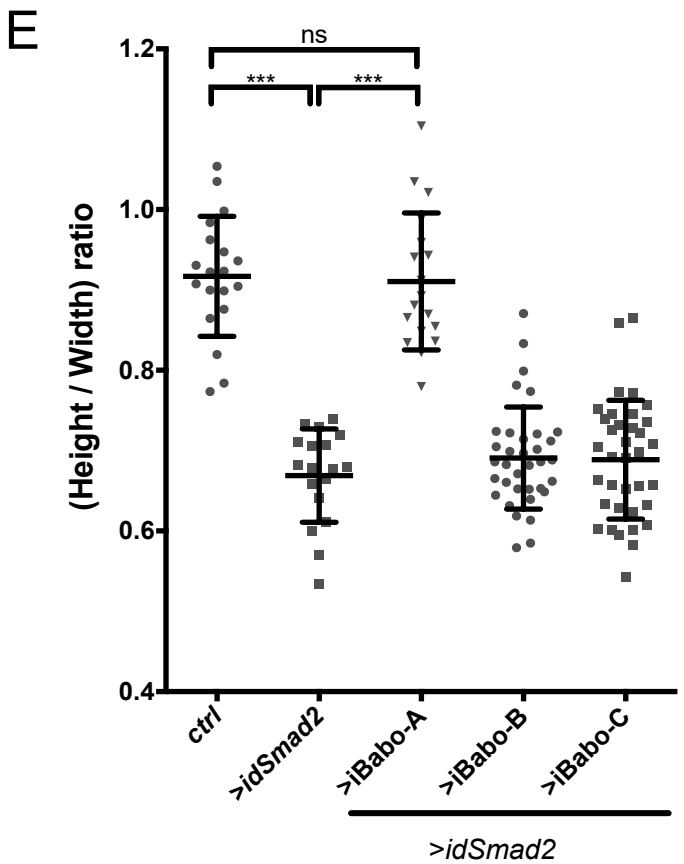

Figure S4

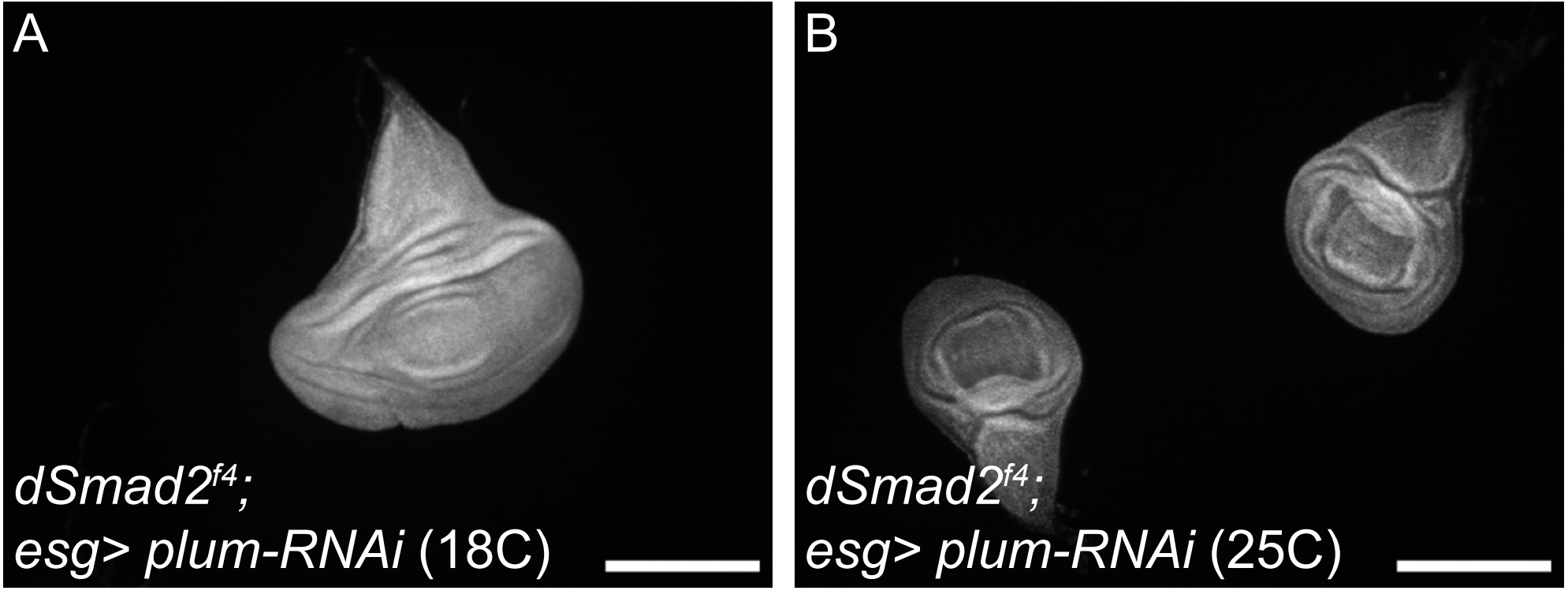

figure S5

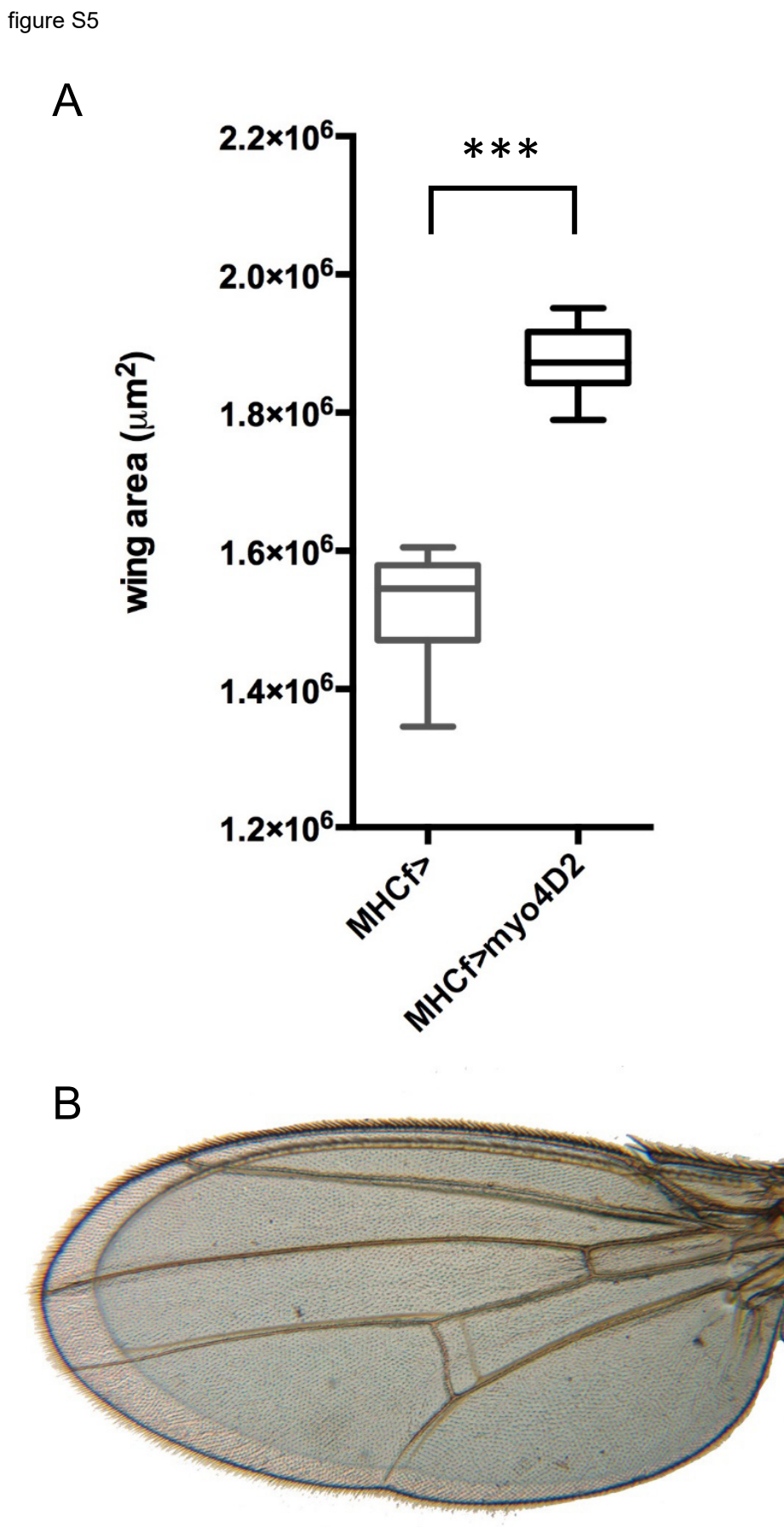
A
2.2×10^6
2.0×10^6
1.8×10^6
1.6×10^6
1.4×10^6
1.2×10^6
wing area (μm^2)
***
MHCf>
MHCf>myo4D2
B